DEVELOPMENT OF AERO-THERMODYNAMIC CYCLE DESIGN CODE FOR TURBOSHAFT ENGINES AND INVESTIGATION OF FOULING EFFECTS ON PERFORMANCE

A THESIS SUBMITTED TO
THE GRADUATE SCHOOL OF NATURAL AND APPLIED SCIENCES
OF
MIDDLE EAST TECHNICAL UNIVERSITY

BY

UMUT SADIKOĞLU

IN PARTIAL FULFILLMENT OF THE REQUIREMENTS
FOR
THE DEGREE OF MASTER OF SCIENCE
IN
MECHANICAL ENGINEERING

AUGUST 2022

Approval of the thesis:

DEVELOPMENT OF AERO-THERMODYNAMIC CYCLE DESIGN CODE FOR TURBOSHAFT ENGINES AND INVESTIGATION OF FOULING EFFECTS ON PERFORMANCE

submitted by **UMUT SADIKOĞLU** in partial fulfillment of the requirements for the degree of **Master of Science in Mechanical Engineering**, **Middle East Technical University** by,

Prof. Dr. Halil Kalıpçılar
Dean, Graduate School of **Natural and Applied Sciences** _____

Prof. Dr. M. A. Sahir Arıkan
Head of the Department, **Mechanical Engineering** _____

Assist. Prof. Dr. Özgür Uğraş Baran
Supervisor, **Mechanical Engineering Dept., METU** _____

Assist. Prof. Dr. Onur Baş
Co-Supervisor, **Mechanical Engineering Dept., TEDU** _____

Examining Committee Members:

Prof. Dr. Sinan Eyi
Aerospace Engineering Dept., METU _____

Assist. Prof. Dr. Özgür Uğraş Baran
Supervisor, Mechanical Engineering Dept., METU _____

Assist. Prof. Dr. Onur Baş
Co-Supervisor, Mechanical Engineering Dept., TEDU _____

Assist. Prof. Dr. Hediye Atik
Aerospace Engineering Dept., Atılım Uni. _____

Assist. Prof. Dr. Ali Karakuş
Mechanical Engineering Dept., METU _____

Date: 04.08.2022

I hereby declare that all information in this document has been obtained and presented in accordance with academic rules and ethical conduct. I also declare that, as required by these rules and conduct, I have fully cited and referenced all material and results that are not original to this work.

Name Last name : Umut Sadıkoğlu

Signature :

ABSTRACT

DEVELOPMENT OF AERO-THERMODYNAMIC CYCLE DESIGN CODE FOR TURBOSHAFT ENGINES AND INVESTIGATION OF FOULING EFFECTS ON PERFORMANCE

Sadıkoğlu, Umut
Master of Science, Mechanical Engineering
Supervisor: Assist. Prof. Dr. Özgür Uğraş Baran
Co-Supervisor: Assist. Prof. Dr. Onur Baş

August 2022, 107 pages

In this thesis, a turboshaft engine performance analysis code is developed on MATLAB. Furthermore, compressor map generation from limited data and deterioration effects on the engine performance are investigated. It is considered that the first step of designing a gas turbine is the selection of the aero-thermodynamic cycle. For this purpose, design point analysis with the parametric design capability is conducted and engine limits are determined. Subsequently, off-design analyses are initiated. During the off-design analyses, component performance maps are scaled according to the design point analysis results. Construction of the performance maps is followed by determining the matching points of the components with varying operating conditions. Then, the engine performance during transitions is examined using the polar moments of inertia of the components and fuel flow outputs of the off-design analyses. Steady-state and transient performance analyses mentioned up to this point is verified by GasTurb 14. For the validation of the code, the General Electric T700 engine is chosen. The developed code is then combined with the compressor performance map generation method called stage-stacking. The General Electric LM2500-30 engine is used for the stage stacking algorithm due to access to

its running line and flow field geometry data. Lastly, stage fouling effects on the performance parameters are evaluated for the compressor section. For this purpose, a modified version of the method suggested by MacIsaac is used. Once the clean and fouled maps of the compressor are obtained, steady-state and transient performance analyses are performed to assess the effect of compressor fouling on overall engine performance.

Keywords: Helicopter Turboshaft Engine, Gas Turbine Performance Modeling, Thermodynamic Matching Model, Gas Turbine Performance Deterioration, Stage-Stacking Technique

ÖZ

TURBOŞAFT MOTORLAR İÇİN ÇEVRİM KODU TASARLANMASI VE KİRLENMENİN PERFORMANS ÜZERİNDEKİ ETKİLERİNİN İNCELENMESİ

Sadıkoğlu, Umut
Yüksek Lisans, Makina Mühendisliği
Tez Yöneticisi: Dr. Öğr. Üyesi Özgür Uğraş Baran
Ortak Tez Yöneticisi: Dr. Öğr. Üyesi Onur Baş

Ağustos 2022, 107 sayfa

Bu tezde, MATLAB programı kullanılarak turboşaft motor performans analiz kodu geliştirilmiştir. Ayrıca, kısıtlı bir veri setini kullanarak kompresör performans haritası üretimiyle birlikte kompresör bölümünde oluşacak kirlenmenin motor bütünündeki performans etkisi incelenmiştir. Bir gaz türbinli motor tasarlamanın ilk adımının aero-termodinamik çevrimin seçimi olduğu görülmüş ve bu doğrultuda parametrik tasarım da yapabilen bir tasarım noktası analiz modülü tasarlanmıştır. Tasarlanan bu modülün kullanımı sayesinde motorun kabiliyetleri ve limitleri belirlenmiştir. Bir sonraki aşama olan tasarım dışı noktalarda motorun denge durumu performansının incelenmesi için yeni bir modül tasarlanmış ve kompresör ile gaz türbinini bağlayan şaftın farklı hızları için analizler yapılarak motorun çalışma zarfındaki davranışı analiz edilmiştir. Bu analizler sırasında kompresör ve türbünlerin performans haritaları ölçeklendirilerek kullanılmıştır. Bu analizlerin tamamlanmasının ardından dinamik davranış analiz çalışmaları başlatılmıştır. Bu analizler sırasında motorun zamana bağlı davranışı incelenip, motor bileşenlerinin eylemsizlik momentleri de dikkate alınmıştır. Buraya kadar bahsedilen denge ve

dinamik durum analizleri GasTurb 14 yazılımı kullanılarak doğrulanmıştır. Elde edilen çıktılar aynı zamanda literatürde yer alan General Electric T700 bilgileriyle de karşılaştırılıp doğrulanmıştır. Tüm bunlara ek olarak, literatürde sıkça görülen kompresör performans haritasının eksikliği nedeniyle bir kompresör haritası oluşturma tekniği olan kademe istifleme yöntemi koda eklenmiştir. Kademe istifleme yönteminde, kompresör kademelerinin genelleştirilmiş özellikleri dikkate alınarak kompresör performans haritası oluşturulmuştur. Kademe istifleme yönteminin kullanılması amacıyla General Electric LM2500-30 motoru ele alınmıştır. Bu metod sayesinde oluşturulan kompresör haritasına, MacIsaac tarafından önerilen modelin birtakım modifikasyonlar ile uygulanması ardından kirlenme etkisinde ortaya çıkacak harita belirlenmiştir. Kirli ve temiz haritalar elde edildikten sonra ise kompresör bileşenindeki kirlenmenin motorun tamamında oluşturacağı denge durumu ve dinamik etkisi analiz edilmiştir.

Anahtar Kelimeler: Helikopter Turboşaft Motorları, Gaz Türbinli Motorların Performans Analizi, Termodinamik Eşleşme Modeli, Gaz Türbinli Motorlarda Performans Düşüşü, Kompresör Kademesi İstifleme Yöntemi

Dedicated to my family...

ACKNOWLEDGMENTS

Firstly, I would like to express my gratitude to Dr. Ö. Uğraş Baran and Dr. Onur Baş for their guidance, advice, criticism, encouragements, and insight throughout the research.

I would also like to thank Yüksel Ortakaya, Alper Ezertaş, Kerem Denk, and Gökhan Aslan for their kindly support and guidance.

I would also like to thank to my colleagues and friends for their friendship, support, inspiring technical discussions, and aid in the proofreading of this thesis.

I would specially thank to Mert Erk, who inspires me to study on gas turbine performance, for his academical and mental support.

I want to express my deepest thanks to my parents Süreyya Sadıkoğlu, Ercüment Sadıkoğlu and sister Gökçe Sadıkoğlu for their spiritual support.

I devote this thesis to my beloved soul mate Pınar Özek, who never stop believing and supporting me.

TABLE OF CONTENTS

LIST OF TABLES

TABLES

LIST OF FIGURES

FIGURES

LIST OF ABBREVIATIONS

FS	Fouling Severity Factor
GE	General Electric
I,J	Polar Moment of Inertia
ISA	International Standard Atmosphere
K	Kelvin
N	Rotational Speed of Component
RPM	Revolution per Minute
GGT, GT	Gas Generator Turbine
PT	Power Turbine
FADEC	Full Authority Digital Engine Control
FOD	Foreign Object Damage
HPT	High Pressure Turbine
LPT	Low Pressure Turbine
VIGV	Variable Inlet Guide Vane

LIST OF SYMBOLS

Symbols

V, C	Flow Velocity
ω	Angular Speed of Rotating Shaft
A	Area
β	Bleed Air Percentage, Beta value
ρ	Density
η	Efficiency
τ	Enthalpy Ratio, Temperature Ratio
S	Entropy
ϕ	Flow Coefficient
f	Fuel-Air Ratio, Function
$\dot{Q}$	Heat Transfer Rate
LHV	Lower Heating Value
M	Mach Number
$\dot{m}$	Mass Flow Rate
$\dot{W}$	Power
P	Pressure
π, PR	Pressure Ratio
ψ	Pressure Rise Coefficient
γ	Ratio Of the Specific Heats, Pressure Loss
N	Rotational Speed
h	Specific Enthalpy
SFC	Specific Fuel Consumption
c_p	Specific Heat Capacity
a	Speed of Sound, Absolute Flow Angle
r	Stage Inlet Midspan Radius

u	Tangential Blade Speed
T	Temperature
φ	Temperature Dependent Portion of Entropy
ζ	Temperature Rise Coefficient
UPW	Unbalanced Power
R	Universal Gas Constant
W	Work, Watt
δ	$P/101.325$ Kpa
θ	$T/288.15$ K

Subscripts

$ambient$	Ambient
$burner$	Burner/Combustion Chamber
c	Compressor
con	Connecting Shaft
$Cooling$	Cooling Flow
$cycle$	Cycle
des	Design Point Value
$diff$	Diffuser
e	Exhaust
$exit$	Exit of the Component
ext_{shaft}	Extraction Shaft
f	Fouled Stage Property
$fuel$	Fuel
ggt, g	Gas Generator Turbine, High-Pressure Turbine, Compressor Turbine
g	Global Factor
x	Axial Direction
$inlet$	Inlet of the Component
$isen$	Isentropic
map	Map Scaling Point
max	Maximum
min	Minimum
$nozzle$	Nozzle
∞	Polytropic
PT	Power Turbine, Free Turbine
ram	Ram

r	Reduced
ref	Reference Value
FS_i	Relative Severity Factor at Stage i
$stage$	Stage Property
$static$	Static Property
$total$	Total Property
t	Turbine, Time

Superscripts

$*$	Generalized Parameter
$'$	Ideal Process

CHAPTER 1

INTRODUCTION

1.1 Gas Turbines and Brayton Cycle

Gas turbines are one of the engine types categorized as internal combustion engines. These engines use air as a working fluid and utilize the chemical energy from burning fuel. Gas turbines are mainly divided into three subsections: compressor, combustion chamber, and turbine. Unlike the other internal combustion engines, compression, combustion, and expansion occur simultaneously in different sections of the engine. Gas turbines are categorized by their architecture and working principles:

1- Turbojet
2- Turbofan
3- Turboprop
4- Turboshaft

The working principle of gas turbine engines is sucking air throughout an engine inlet into the compressor section. Throughout the compressor section, the incoming air pressure increases; hence it is energized. Then, the pressurized air enters the combustion chamber, where the fuel is added to the incoming airflow for combustion process. After the combustion chamber, the highly energized flow is directed to the gas generator turbine (high-pressure turbine). Afterward, the gas generator turbine expands this energized flow and produces work. This work is used for the compressor operation to sustain the cycle. There is always more fuel supply during the cycle to satisfy compressor-gas generator turbine work balance because the primary purpose is to provide usable work. For turboshaft engines, this mechanical energy is obtained from the conversion of the excess energy of fuel combustion by expanding the flow in the power turbine (low-pressure turbine) section. This gained

mechanical power is transferred to the rotors via a transmission system. This engine section makes the difference between the turbojet and turboshaft engines.

This thesis mainly focuses on dual spool turboshaft engines, Figure 1-1 shows the general structure of the engine.

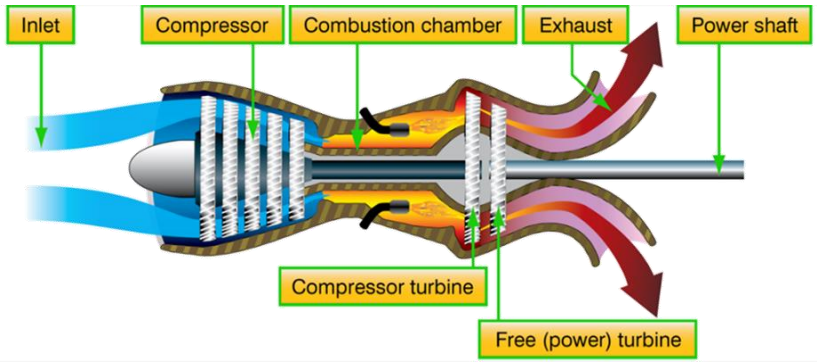

Figure 1-1. Turboshaft Engine Structure [1]

In order to explain and fully understand the working principle of these types of engines, Brayton cycle shall be considered. In this way, working fluid and engine thermodynamic behavior can be understood.

1.1.1 Ideal Brayton Cycle

As mentioned above, the processes of the turboshaft engine are modeled by the Brayton cycle. Related Pressure-Volume (P-V) and Temperature-Entropy (T-S) diagrams are presented in Figure 1-2.

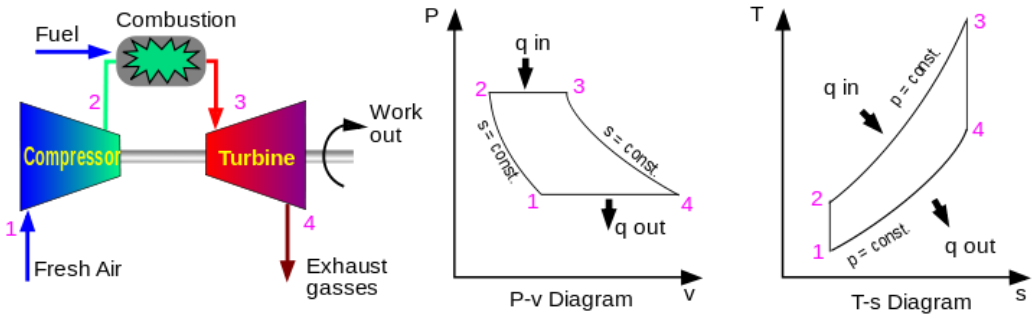

Figure 1-2 P-V and T-S diagrams [2]

Hence, the ideal Brayton Cycle can be summarized as:

- 1-2: Isentropic compression (compressor)
- 2-3: Constant pressure heat addition (combustion chamber/burner)
- 3-4: Isentropic expansion (turbine)
- 4-1: Constant pressure heat rejection

In an ideal Brayton Cycle, the working fluid is considered an ideal gas throughout the cycle, as depicted by Saravanamuttoo et al. [3]. In addition, bleed air, which is pressurized air extracted from the compressor, is not applied for the calculations in this section.

Thus, the powers of the main components, which are the compressor and turbine, are calculated by considering the mass flow rate and enthalpy values at the inlet and outlet of the relevant component.

$$\dot{W}_c = \dot{m}_2\left(h_{total_2} - h_{total_1}\right) \tag{1.1}$$

$$\dot{W}_t = \left(\dot{m}_2 + \dot{m}_{fuel}\right)\left(h_{total_3} - h_{total_4}\right) \tag{1.2}$$

In Equations (1.1) and (1.2), subscripts "c" and "t" represent the compressor and turbine, respectively. The term $\dot{m}$ is used for the mass flow rates and h represents the station's enthalpy value.

The net power of the cycle could be calculated by subtracting the compressor power from the turbine power as given in Equation (1.3):

$$\dot{W}_{cycle} = \dot{W}_t - \dot{W}_c \tag{1.3}$$

In the ideal cycle configuration, the combustion chamber is modeled as a heat and mass source, and the calculation is done by using Equation (1.4):

$$\dot{Q}_{23} = \dot{m}_{fuel} LHV = \left(\dot{m}_2 + \dot{m}_{fuel}\right) h_{total_3} - \dot{m}_2 h_{total_2} \tag{1.4}$$

Where $\dot{Q}_{23}$ stands for heat addition, and LHV is the Lower Heating Value, specific to each fuel type. Overall cycle efficiency can now be determined with Equation (1.5).

$$\eta_{cycle} = \frac{\dot{W}_{cycle}}{\dot{Q}_{23}} = 1 - \frac{\dot{Q}_{in}}{\dot{Q}_{out}} = 1 - \frac{\dot{m} c_p (T_4 - T_1)}{\dot{m} c_p (T_3 - T_2)} = 1 - \frac{T_1}{T_2} \frac{\left(\frac{T_4}{T_1} - 1\right)}{\left(\frac{T_3}{T_2} - 1\right)} \tag{1.5}$$

In Equation (1.5), it is assumed that the fuel flow rate is negligible with respect to the airflow through the engine. Therefore, mass flow rates cancel out each other.

Under the isentropic flow assumptions, the relation given in Equation (1.6) can be implemented into Equation (1.5).

$$T_2/T_1 = \left(P_2/P_1\right)^{\gamma-1/\gamma} = \left(P_3/P_4\right)^{\gamma-1/\gamma} = T_3/T_4 \tag{1.6}$$

Thus, simplifying Equation (1.5) with the help of Equation (1.6), the cycle efficiency in terms of pressure ratios is achieved by using Equation (1.7).

$$\eta_{cycle} = 1 - \left(\frac{1}{P_2/P_1}\right)^{\gamma-1/\gamma} = 1 - \left(\frac{1}{P_3/P_4}\right)^{\gamma-1/\gamma} \tag{1.7}$$

According to these definitions, the relation between pressure ratio and efficiency of a cycle is represented in Figure 1-3.

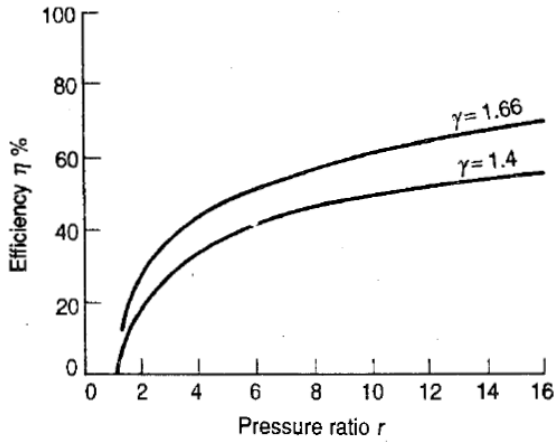

Figure 1-3 Pressure Ratio vs Cycle Efficiency [3]

In addition to considerations that are mentioned up to this point, specific fuel consumption (SFC), which is one of the essential cycle performance parameters, is calculated as in Equation (1.8).

$$SFC = \dot{m}_{fuel} \Big/ \dot{W}_{cycle} \tag{1.8}$$

To investigate actual cycles, The efficiency of the primary components and pressure losses of the flow needs to be considered.

1.1.2 Brayton Cycle with Losses and Efficiency Definitions

The actual Brayton Cycle differs from the ideal Brayton Cycle since the processes are not reversible. The reasons for such losses are listed as follows:

- Since the flow velocities are considerably high through the components, the variation of kinetic energy cannot be neglected. Moreover, the processes are irreversible and assessed as adiabatic; therefore, entropy increases, especially during the expansion and compression processes.

- Pressure losses that caused by the friction between the working fluid and the walls of the components, which are the combustion chamber, inlet, and exhaust duct. In addition, components used for mechanical energy transfer, shafts, and mechanical fittings, also lead to frictional losses.
- Effect of pressure, temperature, and chemical composition of the working fluid results in a variation on c_p and γ.
- In contrast to the ideal cycle, compressor efficiency, combustion chamber efficiency, and turbine efficiency should be taken into account.

Stagnation (total) properties should be investigated in order to evaluate these losses and efficiencies.

1.1.2.1 Stagnation Properties

The concept of stagnation or total enthalpy comes into prominence when the kinetic energy is taken into account for the energy equation with steady flows since the velocity and enthalpy are both assessed in stagnation enthalpy. In detail, the stagnation enthalpy, h_0, is a combination of enthalpy, h, and velocity, C, when the flow is brought to rest with no work and heat transfer. So, the energy equation can be written as in Equation (1.9).

$$(h_0 - h) + \frac{1}{2}(0 - C^2) = 0 \tag{1.9}$$

In Equation (1.9), h_0 is defined as in Equation (1.10).

$$h_0 = h + {C^2}/{2} \tag{1.10}$$

If the fluid is an ideal gas, then c_pT could be replaced by h. Arranging Equation (1.10), the stagnation temperature can be calculated as in Equation (1.11).

$$T_0 = T + {C^2}/{2c_p} \tag{1.11}$$

The term ${C^2}/{2c_p}$ in Equation (1.11) is the dynamic temperature, and T is the static temperature.

Under the assumption of adiabatic compression, work per unit mass flow is calculated by using Equation (1.12).

$$W = -c_p(T_2 - T_1) - {1}/{2}\,(C_2^2 - C_1^2) = -c_p(T_{02} - T_{01}) \tag{1.12}$$

With no work transfer, heat per unit mass flow is calculated with Equation (1.13).

$$Q = c_p(T_{02} - T_{01}) \tag{1.13}$$

As can be deduced from the above equations, if the stagnation properties are used, there is no need to use the kinetic energy term.

Assuming that the process is isentropic as well being adiabatic, another important parameter, the stagnation pressure, is defined in Equation (1.14).

$${P_0}/{P} = \left({T_0}/{T}\right)^{{\gamma}/{\gamma-1}} \tag{1.14}$$

Substituting Equation (1.11) into Equation (1.14) and inserting the $P = \rho RT$ and $c_p = {\gamma R}/{(\gamma - 1)}$ relations, the stagnation pressure can be calculated with Equation (1.15).

$$P_0 = P\left(1 + \frac{\rho C^2}{2P} \cdot \frac{\gamma - 1}{\gamma}\right)^{{\gamma}/{\gamma-1}} \tag{1.15}$$

Moreover, under the assumption of isentropic compression through the compressor, Equation (1.14) can be written in the form given in Equation (1.16):

$$P_{02}/P_{01} = P_{02}/P_2 \cdot P_1/P_{01} \cdot P_2/P_1 = \left(T_{02}/T_2 \cdot T_1/T_{01} \cdot T_2/T_1\right)^{\gamma/\gamma-1} \quad (1.16)$$
$$= \left(T_{02}/T_{01}\right)^{\gamma/\gamma-1}$$

Thus, stagnation properties can be approached similarly to static properties, assuming an isentropic process. A similar procedure is also applicable for the expansion processes.

With all the considerations discussed until this point, representative T-S diagrams in Figure 1-4 are achieved for the compressor and turbine, which indicate the difference between static and stagnation properties.

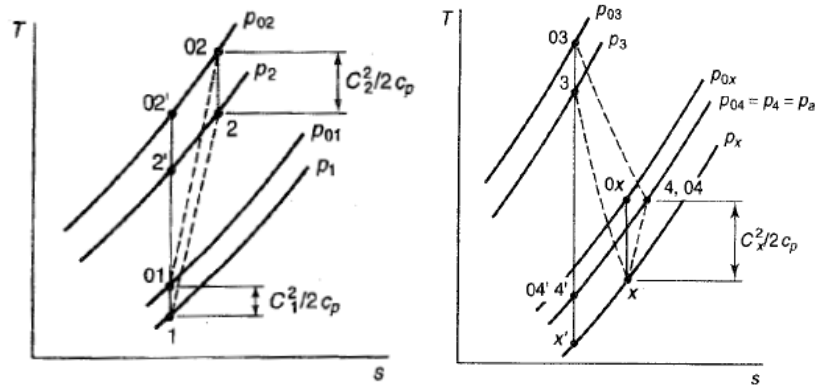

Figure 1-4 T-S Diagram with Stagnation Values – Compressor (Left) & Turbine (Right) [3]

1.1.2.2 Efficiencies of Compressors and Turbines

The efficiency of any machine can be defined as the division of actual work into ideal work. Since the ideal work is isentropic, the main components' efficiencies are defined as isentropic efficiency. Applying the concept of stagnation properties discussed in Chapter 1.1.2.1, Equations (1.17) and (1.18) are derived for isentropic efficiencies. Primes in the equations indicate the ideal state properties.

$$\eta_c = W'/W = \Delta h_0'/\Delta h_0 = T_{02}' - T_{01}/T_{02} - T_{01} \quad (1.17)$$

$$\eta_t = {W}/{W'} = {T_{03} - T_{04}}/{T_{03} - T'_{04}} \tag{1.18}$$

Once the efficiencies are calculated, temperature variation is determined with the given pressure ratio. Subsequently, the change in the temperatures at the inlet and exit of the components are calculated with Equations (1.19) and (1.20).

$$T_{02} - T_{01} = {T_{01}}/{\eta_c}\left[\left({P_{02}}/{P_{01}}\right)^{{\gamma-1}/{\gamma}} - 1\right] \tag{1.19}$$

$$T_{03} - T_{04} = \eta_t T_{03}\left[1 - \left(\frac{1}{P_{03}/P_{04}}\right)^{{\gamma-1}/{\gamma}}\right] \tag{1.20}$$

In general, compressors and turbines are in cascade form (consist of multiple stages). Isentropic efficiencies for these components are generally assumed to be constant for the whole cascaded component. However, proceeding with this assumption for cycle analysis is not realistic. It is known that compressor efficiency decreases, and turbine efficiency increases with the increasing pressure ratio for which the component is designed. Therefore, polytropic efficiency is defined to eliminate this kind of confusion in the characteristics of the components. By using polytropic efficiency, the whole component is studied stage by stage in contrast to isentropic efficiency.

The blade profile is assumed to be similar through the stages for compressors. So, the stage compressor efficiency, η_{stage}, will remain constant for the rest of the component. Thus, Equation (1.21) is used for the overall component efficiency calculations.

$$\Delta T = \Sigma {\Delta T'_{stage}}/{\eta_{stage}} = {1}/{\eta_{stage}}\,\Sigma \Delta T'_{stage} \tag{1.21}$$

Implementing $\Delta T = {\Delta T'}/{\eta_c}$ to Equation (1.21), the relation between stage and overall efficiency is determined as given in Equation (1.22):

$$\eta_{stage}/\eta_c = {\Sigma\Delta T'_{stage}}/{\Delta T'} \tag{1.22}$$

With the increasing entropy value, the difference between the constant pressure lines increases, resulting in $\Sigma\Delta T'_{stage} > \Delta T'$(see Figure 1-5). Thus, it can be concluded that $\eta_c < \eta_{stage}$. The difference between η_c and η_{stage} increases with the number of stages. For the turbines, the relation appears as $\eta_t > \eta_{stage}$.

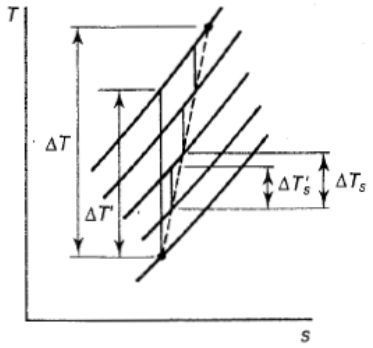

Figure 1-5 Comparison of Stage by Stage and Total Temperature Rises [3]

These approaches lead to the determination of polytropic efficiency, η_∞, which can be defined as stage isentropic efficiency. The polytropic efficiency for the compressor is given in Equation (1.23):

$$\eta_{\infty c} = {dT'}/{dT} \tag{1.23}$$

For an isentropic process, ${T}/{P^{\gamma-1/\gamma}}$ term is constant and can be differentiated as in Equation (1.24).

$$dT'/T = {\gamma - 1}/{\gamma} \,.\, dP/P \tag{1.24}$$

Implementing Equation (1.23) into (1.24), results in Equation (1.25).

$$\eta_{\infty c}\, dT/T = {\gamma - 1}/{\gamma} \cdot dP/P \tag{1.25}$$

By integrating Equation (1.25) between inlet (1) and exit (2) of the compressor, Equation (1.26) is achieved.

$$\eta_{\infty c} = \left. ln\left({}^{P_2}/_{P_1}\right)^{\frac{\gamma-1}{\gamma}} \right/ ln\left({}^{T_2}/_{T_1}\right) \tag{1.26}$$

Thus, temperature and pressure ratio through the compressor can be written as in Equation (1.27):

$${}^{T_2}/_{T_1} = \left({}^{P_2}/_{P_1}\right)^{\frac{\gamma-1}{\gamma\eta_{\infty c}}} \tag{1.27}$$

Afterward, $\eta_{\infty c}$ and η_c can be related to each other by using Equation (1.28).

$$\eta_c = \frac{{}^{T_2'}/_{T_1} - 1}{{}^{T_2}/_{T_1} - 1} = \frac{\left({}^{P_2}/_{P_1}\right)^{{}^{\gamma-1}/_{\gamma}} - 1}{\left({}^{P_2}/_{P_1}\right)^{{}^{\gamma-1}/_{\gamma\eta_{\infty c}}} - 1} \tag{1.28}$$

For the turbines, polytropic efficiency is defined in Equation (1.29).

$$\eta_{\infty t} = {}^{dT}/_{dT'} \tag{1.29}$$

With Equation (1.30), the relation between pressure and temperature ratio through the turbine in terms of polytropic efficiency is determined.

$${}^{T_3}/_{T_4} = \left({}^{P_3}/_{P_4}\right)^{\frac{\eta_{\infty t}(\gamma-1)}{\gamma}} \tag{1.30}$$

And $\eta_{\infty t}$ and η_t can be related to each other by using Equation (1.31).

$$\eta_t = \frac{1 - \left(\frac{1}{P_3/P_4}\right)^{\eta_{\omega t}(\gamma-1)/\gamma}}{1 - \left(\frac{1}{P_3/P_4}\right)^{(\gamma-1)/\gamma}} \tag{1.31}$$

1.2 Descriptions and Configurations of Components

The main components listed below shall be understood and studied very well to understand the characteristics of the gas turbines and analyse the behavior of the engines in various conditions:

- Inlet
- Compressor
- Combustion Chamber (Burner)
- Turbine
- Exhaust

A typical turboshaft engine structure and the main components which are listed above are represented in Figure 1-1. Representative station numberings per component are given in Figure 2-1.

1.2.1 Inlet

Inlets are the primary components that the incoming air encounters and are used to transform the kinetic energy of the freestream airflow or forward velocity into the total pressure and temperature. Considering the Bernoulli Theorem, for relatively low speeds, the inlet diffuses the incoming air (the velocity of the incoming air is reduced while the pressure of the air is increased) to achieve a more efficient compressor operation, which means that the inlets are designed for minimum pressure loss.

1.2.2 Compressor

The compressor is a component that energizes the incoming air from the inlet by pressurizing it. As it may be concluded from Figure 1-3, the increase in the pressure ratio of the compressor increases the thermal efficiency of the Brayton Cycle. More compressor stages are required to increase the pressure ratio of the compressor. This increase leads to more losses because of the frictional and mechanical effects. Also, this leads to an increase in the weight and complexity of the engine.

1.2.2.1 Design Configurations of Compressors

Compressors are separated into three types according to their structure:

- Axial compressors
- Centrifugal compressors
- Axial-Centrifugal compressor

The types that are listed above are briefly described in the following subsections.

1.2.2.1.1 Axial Compressor

For an axial compressor, the rotation axis is parallel to the airflow. Axial compressors consist of several airfoils in a row. These rows are separated into two categories called rotor blades and stator vanes. The rotor blades are attached to the gas generator shaft, which connects the compressor and gas generator turbine (the turbine that is used to sustain compressor operation) sections, rotating at high speeds. Throughout the operation, incoming air is accelerated by the rotation of rotor blades and directed onto the stator vanes. In the stationary stator vanes, air is diffused, and the kinetic energy of the flow is converted into pressure. Stator vanes also deflect the incoming air at an appropriate angle for the next stage The stator vanes located at the end of the compressor section are designed to straighten the airflow and remove the swirl [4]. According to Flack [5], one stage of an axial compressor generally supplies

the pressure ratio from 1.15 to 1.28. Hence, multiple rows are needed to provide the required pressure ratio to satisfy the cycle. The representation of a typical axial compressor is given in Figure 1-6.

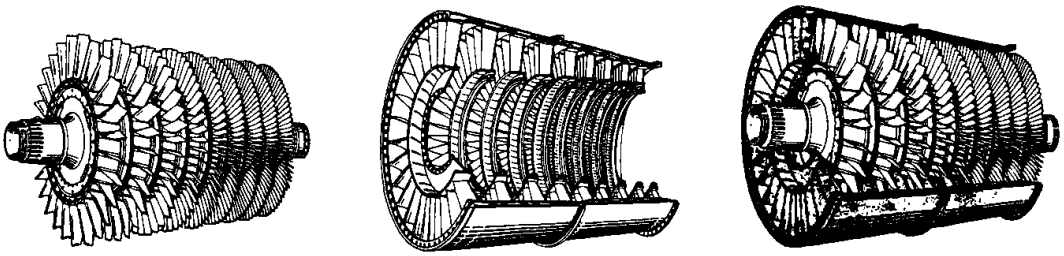

Figure 1-6 Typical Axial Compressor [6]

Also, the variation of pressure and velocity through the flow pattern of the air is given in Figure 1-7.

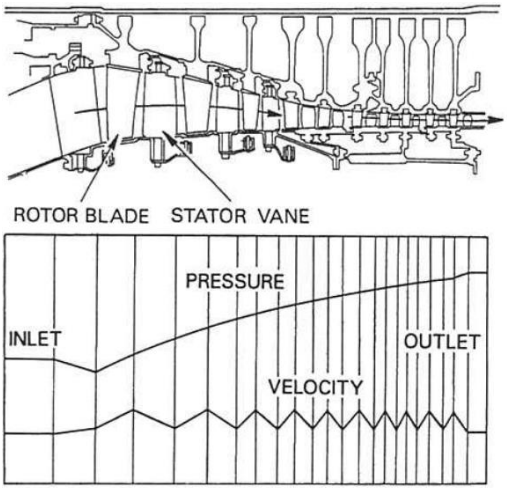

Figure 1-7 Pressure and Velocity Variation Through Flow Pattern of the Axial Compressor [4]

1.2.2.1.2 Centrifugal (Radial) Compressor

The axis of rotation is perpendicular to the air outflow for the centrifugal compressors. Centrifugal compressors have mainly three components, as shown in Figure 1-8.

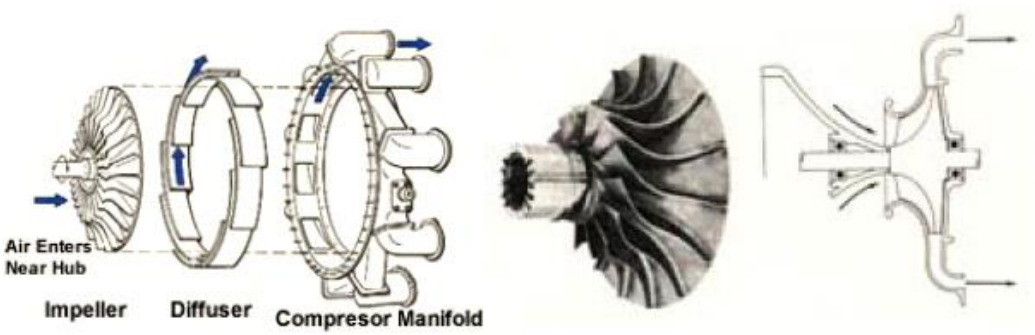

Figure 1-8 Centrifugal Compressor Illustration [7]

These components are listed as:

- Impeller
- Diffuser
- Compressor manifold

In detail, the impeller is the rotational component of the compressor. The incoming airflow, which has no vorticity, encounters the rotating impeller. As the flow passes through the impeller, due to the centrifugal force occurred by the rotation, it is directed outward.

Then, the air leaving the impeller flows to a stationary section called the diffuser. In the diffuser, the air is expanded through diverging channels. Thus, the diffuser reduces the flow velocity and increases the pressure of the flow.

Finally, the manifold discharges the air to another compressor stage or combustion chamber to accomplish the combustion process.

Representative pressure and velocity variation through the centrifugal compressor is given in Figure 1-9.

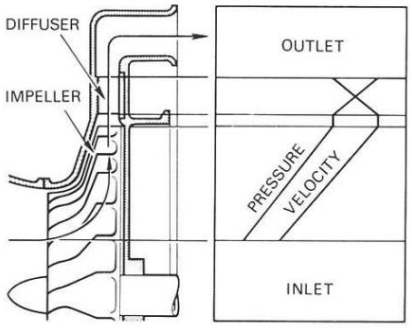

Figure 1-9 Pressure and Velocity Variation Through Flow Pattern of the Centrifugal Compressor [4]

1.2.2.1.3 Axial-Centrifugal Compressor

A combination of axial and centrifugal compressors may give a better result for some applications. This combination results in the utilization of advantages of each compressor type. Axial-centrifugal compressor generally consists of a series of axial compressor stages followed by a single stage of a centrifugal compressor. This configuration minimizes the frontal area that comes with the advantage of an axial compressor and reduces the manufacturing limitations caused by the smaller area at the last stage of an axial compressor by connecting it to the centrifugal compressor. The structure of the axial-centrifugal compressor is represented in Figure 1-10.

Figure 1-10 Axial-Centrifugal Compressor [8]

1.2.3 Combustion Chamber (Burner)

The combustion chamber is a section where the burning process takes place. The incoming pressurized air from the compressor section mixes with the fuel in the combustion chamber. Due to this, the core flow is energized with the addition of fuel. Thus, the chemical energy is converted to thermal energy. Ideally, combustion is assumed as a constant pressure process. However, in actual cases, there are pressure losses and not all of the supplied fuel burns. While designing the combustion chamber, the effectiveness of the section is specified by considering the following properties:

- Combustion efficiency (amount of burnt fuel divided by the amount of supplied fuel)
- Pressure loss through the combustion chamber
- Stability of the combustion chamber
- Temperature distribution at the exit
- The volume of the combustion chamber section
- Operational envelope
- In-flight relight capability

1.2.3.1 Design Configurations of Combustion Chambers

Combustion chambers are categorized commonly as:

- Can combustion chamber
- Annular combustion chamber
- Can-annular combustion chamber

The types that are listed above are briefly described in the following sections.

1.2.3.1.1 Can Combustion Chamber

The design of can combustion chambers contains single or multiple cylindrical burners located at the casing of the engine. The air incoming from the compressor section is divided into each can. These combustion chamber sections have their own fuel injection ports fed from a common fuel supply. Like fuel injection ports, secondary cooling flow is separated into each individual can. They are highly compatible with the centrifugal type of compressors since the compressor manifold separates the pressurized air into channels connected with these cans [9]. Can combustion chamber is represented in Figure 1-11.

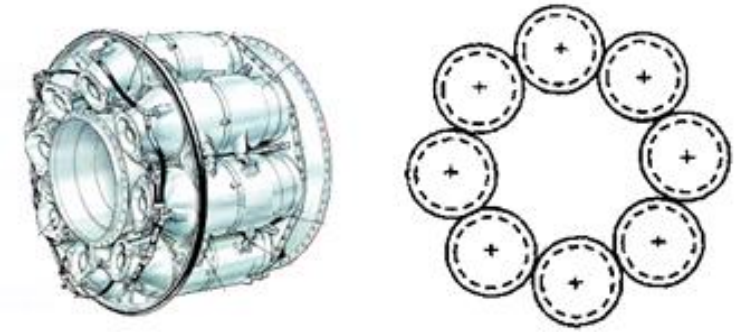

Figure 1-11 Can Combustion Chamber with Cross Sectional View [6] [11]

1.2.3.1.2 Annular Combustion Chamber

In this configuration, both the air ducts and flame tubes are annular. These combustion chambers are very efficient due to their low-pressure loss characteristics [10]. They are also small-sized and provide an efficient ignition due to uniform combustion. However, maintenance operations are challenging since the burning process is not separated into cans. Annular combustion chambers are more effectively used with axial compressors. Figure 1-12 represents the annular combustion chamber.

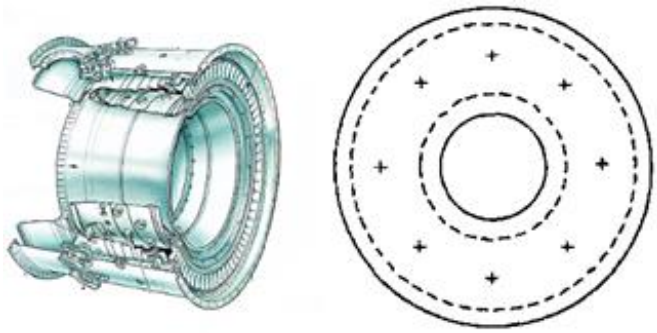

Figure 1-12 Annular Combustion Chamber with Cross Sectional View [6][11]

1.2.3.1.3 Can-Annular Combustion Chamber

The merge of a can and annular combustion chambers form this type of chamber. There is a uniform placement of flame tubes around the annular casing. Unlike the can combustion chambers, all cans have a common cooling flow, such that all cans share a common annulus. A reverse flow pattern from the compressor is utilized in this configuration. The structure of these combustion chambers is shown in Figure 1-13.

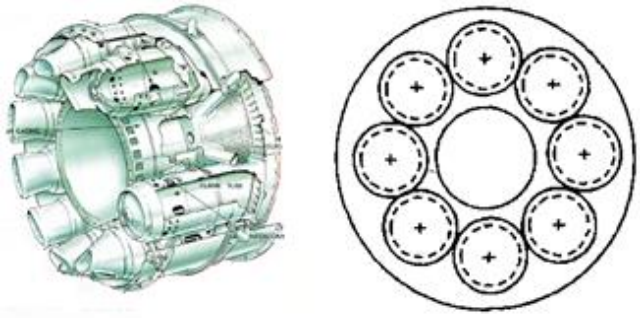

Figure 1-13 Can-Annular Combustion Chamber with Cross Sectional View [6][11]

1.2.4 Turbine

Turbines are compressor-like structures; however, their operating principle is the opposite. They are used to obtain the mechanical work from the energy of the flow. Most of the received mechanical work is used for the compressor operation to sustain

the cycle. The rest of work is used to produce the shaft work for turboshaft engines. During the expansion process, both temperature and pressure drop, leading to a more efficient operation because turbine blades can resist higher aerodynamic loadings. Therefore, fewer stages are required for turbines than for compressors.

Since the gas generator turbine is located after the combustion chamber, the incoming air-fuel mixture is highly energized, and the temperature of the flow is extremely high. When these are combined with the high rotational speed of the turbine, material requirements for design may be challenging. The exact considerations are also valid for power turbines. Turbines differentiate from compressors because the limiting factor is the integrity of their structure rather than their aerodynamics.

1.2.4.1 Design Configurations of Turbines

Turbines typically have two different configurations:

- Axial turbines
- Radial turbines

The types that are listed above are briefly described in the following sections.

1.2.4.1.1 Axial turbines

Axial turbines are highly similar to axial compressors. Unlike the axial compressor, flow first encounters the stationary stator vanes and then rotor blades. A single turbine stage is formed by a single row of stator vanes and rotor blades. These types of turbines are primarily divided into two categories as impulse turbines and reaction turbines. Figure 1-14 represents the difference in blade profiles of these two types.

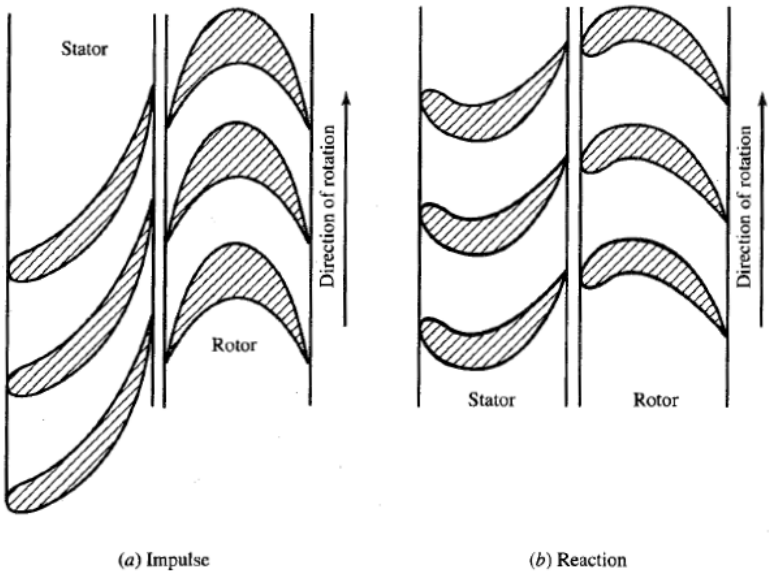

Figure 1-14 Impulse and Reaction Turbines [6]

For the impulse turbines, the relative velocity at the exit of the rotor is nearly the same as the relative velocity at the rotor inlet. There is no significant pressure change through the rotor. The profile of stator blades is designed to increase the velocity and decrease the pressure at the stator exit.

For the reaction turbines, relative velocity increases through the rotor while the pressure decreases. The stator section is designed to direct the flow through the desired direction, and there is no significant effect on the flow's velocity and pressure.

1.2.4.1.2 Radial Turbine

Radial turbines are very similar to radial compressors. The axial compressor-turbine relations are also valid for the radial compressor-turbine pair. Despite higher pressure ratio characteristics, these turbines are limited with relatively low flow rates, similar to the radial compressors. Because of that, the use of the radial turbine depends on the engine size and requirements, which means if the designed engine is small and operates with lower airflow, the radial turbine may be used.

1.2.5 Exhaust

One of the essential components of a gas turbine is the exhaust. The exhaust system of a turboshaft engine discharges incoming high-temperature flow from the power turbine section. Additionally, it has a significant effect on engine performance and stability. Exhaust systems generally have a nozzle and an ejector (tailpipe). The nozzle directs exhaust gases produced by the engine to the exit of the nacelle with the help of the ejector. Moreover, it also has significant effects on:

- Cooling flow generation
- Back pressure near the turbine exit
- Mixing performance of the exhaust gases and airflow in the outward direction.

The exhaust flow generates the cooling airflow. The low-pressure and high-velocity flow near the turbine exit plane behaves like a venturi. With the help of this, the necessary cooling flow for the engine bay can be directed through cooling air inlets on engine cowlings.

In general, it can be said that the cooling mass flow rate is increased by decreasing the exit cross-sectional area of the nozzle with a constant ejector area.

The nozzle exit area is another point of consideration during the exhaust system design process since it affects turbine exit back pressure, which leads to performance loss and an increase in SFC. When the area is increased, both SFC and available power are increased and vice versa. The main aim is to provide high power with minimum SFC.

1.3 Aero-Thermodynamic Cycle Analysis

Designing a gas turbine begins with determining the requirements and specifications obtained from the market and customer. While determining these specifications, constraints and mission analysis of the aircraft are considered. These specifications

determine the required power/thrust and fuel consumption, which are the leading performance parameters of the gas turbine cycle. Other factors such as weight, volume, cost, and lifespan are secondary specifications that affect the design. Then, the engine design procedure is followed by aero-thermodynamic cycle analysis, which consists of design point and off-design analysis. Design point analysis determines engine performances with different design decisions (e.g., compressor pressure ratio) and limits (e.g., combustion chamber exit temperature). The off-design analysis phase is performed to obtain the performance of a particular engine in the specified operational envelope and power settings. Therefore, these analyses are linked to each other and performed to observe if the engine is capable of supplying the required power with a given fuel flow. As a next step of the design processes, components' aerodynamical and mechanical design are considered. These engine design process phases are iterative and are performed until the requirements mentioned above are satisfied.

Aero-thermodynamical cycle analyses are essential for the preliminary engine design process and must be performed accurately to determine desired engine performance. While performing these analyses, an air model shall be introduced to determine the fluid properties through the engine stations, and flow is considered 1-D. Moreover, the efficiency of each component is considered non-ideal.

1.3.1 Gas Turbine Performance Simulation Models

There are plenty of gas turbine modeling techniques in the literature; each has its own different advantages and disadvantages. However, some of them are more commonly used models when compared to other models, according to Walsh and Fletcher [12]. These particular models are listed below:

- Thermodynamic matching transient performance and control model
- Real-time aerothermal transient performance model
- Real-time transfer function transient performance model

- Real-time lumped parameter transient performance model

Detailed descriptions, usage areas, block diagrams, and comparisons of these models are given in [12], [13], and [14]. Among these models, thermodynamic matching transient performance has the highest accuracy and relatively lower complexity, as stated by Thirunavukarasu [15]. Therefore, throughout the development of the code, it is chosen as the reference type of the modeling technique.

Kurzke, Saravanamuttoo, Walsh, and Fletcher are the most widely cited researchers in the thermodynamic matching model. These researchers have deduced that this method is the most convenient and precise way to estimate gas turbine performance. In Kurzke's studies [16] and [17], fundamental approaches and definitions are given. In addition to these two references, [3], [12], and [18] are other informative publications on gas turbine performance.

During the study, the developed code is verified by comparing the results with the GasTurb software developed by Kurzke. GasTurb is a commercial and widely used software for determining gas turbine performance in both steady-state and transient regimes. GasTurb is chosen as the verification tool because many articles in the literature compare experimental data and model outputs with GasTurb simulation results. These articles are [19], [20], [21], [22], [23]. Therefore, GasTurb is a widely used and proven software for verification purposes.

In addition to comparing the simulation results with the experiments, GasTurb is compared with the other widely used simulation tools such as ASTRA, NPSS, GSP, and EngineSim. It is stated that GasTurb is the most successful program in performing multi-purpose tasks, according to Kuz'michev et al. [24].

1.4 Thesis Outline

The study aims to develop a MATLAB code capable of performing engine performance calculations to examine the fouling effect on performance. For this purpose, steady-state and transient performance analysis code is developed. Then,

the stage-stacking method is adopted and integrated into the developed code to overcome the limited data published by the engine manufacturers and to achieve stage parameters. Construction of the compressor map using the stage-stacking method is followed by the fouling application on the constructed map. In this phase of the study, the fouling algorithm is coupled with the stage-stacking method since fouling is not uniform and varies from stage to stage. With these capabilities, engine preliminary design and investigations of fouling effects on the performance are achieved. In the following, brief information about the contents of the chapters is given.

In Chapter 2, the design point performance calculation method and development of the design point module is explained. Initially, considered turboshaft engine structure and stations of the engine are stated. Since the conceptual engine design is conducted in this phase, high accuracy is needed through the calculations. For this purpose, an air model is developed and integrated to calculate the working fluid properties at the desired engine stations. Development of the air model is followed by on-design, and parametric design modules to compare different design selections and different parameters. This capability of the developed code leads to choosing the most optimum point for the engine's operation. At the end of the chapter, the module results are compared with GasTurb 14 outputs for verification purposes.

In Chapter 3, the off-design performance calculation module is described. Map scaling and the Beta-Line techniques used for determining the component performance are explained. Then, the thermodynamic matching algorithm is described for determining the steady-state engine performance with varying operating conditions and previously determined limitations. After, obtained outputs are verified with the results of GasTurb 14.

In Chapter 4, engine transient performance calculation method is presented. In this module, the engine responses between steady-state thermal equilibrium points are considered. For this purpose, the transient matching algorithm is explained. Through the calculations, Newton-Raphson Algorithm is used, and Euler Integration Method

is considered for the matching and calculations for the next time step. The obtained results are also verified with the GasTurb 14 results.

In Chapter 5, validation model of the developed code by employing the GE T700 engine is described. Design parameters, component maps, and validation methods are explained for steady-state and transient operations.

In Chapter 6, the stage-stacking method to construct a compressor map by considering generalized stage characteristics is explained. For the application of this method, GE LM2500-30 is used because of the flow field geometry and the running line data. The construction of the compressor map is followed by the inclusion of fouling effects on the performance parameters. Therefore, a modified version of the method suggested by MacIsaac is used. After applying the method to the clean engine, performance degradation on the fouled engine is compared with the clean engine.

In Chapter 7, conclusions and future recommendations are given to extend what has been achieved with this study.

For the sake of clarity, the flowchart of the study is given with the diagram in Figure 1-15.

Figure 1-15 Flowchart of the Study

CHAPTER 2

DESIGN POINT PERFORMANCE CALCULATIONS

The design process of an engine begins with a design point performance analysis. This design process contains the conceptual engine design, thermodynamic properties of the working fluid at each station, and performance of the components for a specified application. For these, design point cycle analysis module is developed. Design point analysis computes the engine performance for:

- Design choice (compressor pressure ratio)
- Limiting design parameter (combustion chamber exit temperature)

The following sections briefly describe design point performance calculations using the previously mentioned thermodynamic concepts.

2.1 Station Numbering Regarding the Engine Components

The following calculations are based on a two-spool turboshaft engine. Representations of stations are shown in Figure 2-1.

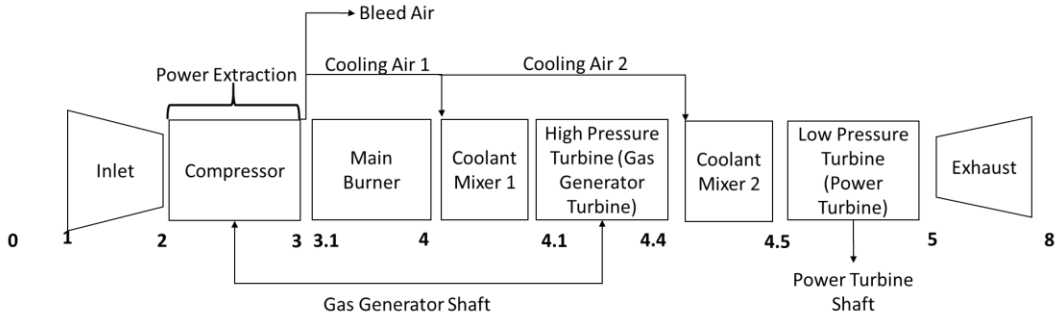

Figure 2-1 Two-Spool Turboshaft Engine with Station Numbers

The process throughout the engine should be represented with the station numbers to emphasize component functions for a better understanding.

In the above diagram, 0 represents the ambient conditions. The entrance of the inlet is marked as 1. Firstly, the air is sucked from 0 to 1. The air loses some energy from stations 1 to 2 because of the inlet losses. Then, incoming air enters the compressor section, which adds energy to the flow (stations 2 to 3). From 3 to 3.1, the section between compressor exit and combustion chamber inlet, bleed extraction takes place and is optional. This extracted bleed can be used in two ways: one is for air-conditioning, and the other is for cooling the turbines to operate more efficiently. Along the combustion chamber section, the fuel is added to the energized air, and the combustion process takes place (sections 3.1 to 4). In the sections between 4 and 4.1, the aforementioned cooling bleed (if any) is fed to the air-fuel mixture to cool down the flow at the inlet of the gas generator turbine. Next, the flow enters the gas generator turbine (stations 4.1 to 4.4) and is expanded to obtain mechanical work for compressor operation. The outflow of the gas generator turbine is again mixed with the cooling flow (stations 4.4 to 4.5) to cool down the inflow of the power turbine. Then, the flow is expanded through the power turbine to obtain the shaft work. Finally, the flow discharges at station 8.

The stations and components are tabulated in Table 2-1.

Table 2-1 Station Numbering and Components

Number of Station	**Component Locations**
0	Ambient / Freestream
1	Inlet Entrance
2	Inlet Exit / Compressor Inlet
3	Compressor Exit
3.1	Combustion Chamber (Burner) Inlet
4	Combustion Chamber Exit
4.1	Gas Generator Turbine Inlet / Cooling Air 1 Supply
4.4	Gas Generator Turbine Exit / Cooling Air 2 Supply
4.5	Power Turbine Inlet
5	Power Turbine Exit
8	Exhaust Nozzle Exit

As mentioned in Section 1.3, the air model was developed to achieve higher accuracies. Since the equations developed for the gas turbine stations are not linear, the use of the ideal gas assumption leads to misleading results. Thus, the developed air model to find the working fluid properties is briefly explained in the following section.

2.2 Working Fluid Property Calculations (Air Model)

First of all, non-dimensional constants to calculate air and air-fuel mixture properties are defined in the code. These constants are achieved via Walsh and Fletcher's book [12]. Table 2-2 and Table 2-3 contain these constants.

Table 2-2 Dry Air Property Constants [12]

$\boldsymbol{A_0}$	0.992313	$\boldsymbol{A_1}$	0.236688
$\boldsymbol{A_2}$	-1.852148	$\boldsymbol{A_3}$	6.083152
$\boldsymbol{A_4}$	-8.893933	$\boldsymbol{A_5}$	7.097112
$\boldsymbol{A_6}$	-3.234725	$\boldsymbol{A_7}$	0.794571
$\boldsymbol{A_8}$	-0.081873	$\boldsymbol{A_9}$	0.422178
$\boldsymbol{A_{10}}$	0.001053		

Table 2-3 Combustion Products of Kerosene Property Constants [12]

$\boldsymbol{B_0}$	-0.718874	$\boldsymbol{B_1}$	8.747481
$\boldsymbol{B_2}$	-15.863157	$\boldsymbol{B_3}$	17.254096
$\boldsymbol{B_4}$	-10.233795	$\boldsymbol{B_5}$	3.081778
$\boldsymbol{B_6}$	-0.361112	$\boldsymbol{B_7}$	-0.003919
$\boldsymbol{B_8}$	0.0555930	$\boldsymbol{B_9}$	-0.0016079

Also, T^* is defined in the code given in Equation (2.1).

$$T^* = {}^{T}/_{1000} \tag{2.1}$$

Because the dynamic temperature is a small portion of the total temperature, calculations of T^* with Mach numbers up to 0.4 could be performed by using total temperature rather than static temperature. In this calculation, the temperature should be in Kelvins.

Using T^* and fuel-air ratio (f), specific enthalpy $\left({}^{kJ}/_{kg}\right)$, h, and specific heat capacity $\left({}^{kJ}/_{kg\,.\,K}\right)$, c_p, of the working fluid are determined with Equations (2.2) and (2.3).

$$\begin{aligned} h = 1000\Bigg(& A_0T^* + \left(\frac{A_1}{2}\right)(T^*)^2 + \left(\frac{A_2}{3}\right)(T^*)^3 + \left(\frac{A_3}{4}\right)(T^*)^4 \\ & + \left(\frac{A_4}{5}\right)(T^*)^5 + \left(\frac{A_5}{6}\right)(T^*)^6 + \left(\frac{A_6}{7}\right)(T^*)^7 \\ & + \left(\frac{A_7}{8}\right)(T^*)^8 + \left(\frac{A_8}{9}\right)(T^*)^9 + A_9 \\ & + \left(\frac{f}{1+f}\right)\Bigg(B_0T^* + \left(\frac{B_1}{2}\right)(T^*)^2 + \left(\frac{B_2}{3}\right)(T^*)^3 \\ & + \left(\frac{B_3}{4}\right)(T^*)^4 + \left(\frac{B_4}{5}\right)(T^*)^5 + \left(\frac{B_5}{6}\right)(T^*)^6 \\ & + \left(\frac{B_6}{7}\right)(T^*)^7 + \left(\frac{B_7}{8}\right)(T^*)^8 + B_8\Bigg)\Bigg) \end{aligned} \tag{2.2}$$

$$\begin{aligned} c_p = {} & A_0 + A_1T^* + A_2(T^*)^2 + A_3(T^*)^3 + A_4(T^*)^4 + A_5(T^*)^5 \\ & + A_6(T^*)^6 + A_7(T^*)^7 + A_8(T^*)^8 \\ & + \left(\frac{f}{1+f}\right)(B_0 + B_1T^* + B_2(T^*)^2 + B_3(T^*)^3 \\ & + B_4(T^*)^4 + B_5(T^*)^5 + B_6(T^*)^6 + B_7(T^*)^7) \end{aligned} \tag{2.3}$$

To calculate the entropy variation through stations, φ shall be defined as in Equation (2.4), which is the temperature-dependent part of entropy.

$$\varphi = \int_{T_{ref}}^{T} {}^{c_p}/_{T}\, dT \tag{2.4}$$

With the assumption of T_{ref} is 0 K, entropies at stations 1 and 2 without integration are achieved by using Equation (2.5):

$$\begin{aligned}\varphi_{1,2} = {} & A_0\, log\left(T_{1,2}\right) + A_1 {T_{1,2}}^* + \left(\frac{A_2}{2}\right)({T_{1,2}}^*)^2 + \left(\frac{A_3}{3}\right)({T_{1,2}}^*)^3 \\ & + \left(\frac{A_4}{4}\right)({T_{1,2}}^*)^4 + \left(\frac{A_5}{5}\right)({T_{1,2}}^*)^5 + \left(\frac{A_6}{6}\right)({T_{1,2}}^*)^6 \\ & + \left(\frac{A_7}{7}\right)({T_{1,2}}^*)^7 + \left(\frac{A_8}{2}\right)({T_{1,2}}^*)^2 + A_{10} \\ & + \left(\frac{f}{1+f}\right)\left(B_0\, log\left(T_{1,2}\right) + B_1 {T_{1,2}}^* + \left(\frac{B_2}{2}\right)({T_{1,2}}^*)^2\right. \\ & + \left(\frac{B_3}{3}\right)({T_{1,2}}^*)^3 + \left(\frac{B_4}{4}\right)({T_{1,2}}^*)^4 + \left(\frac{B_5}{5}\right)({T_{1,2}}^*)^5 \\ & \left. + \left(\frac{B_6}{6}\right)({T_{1,2}}^*)^6 + \left(\frac{B_7}{7}\right)({T_{1,2}}^*)^7 + B_9\right)\end{aligned} \tag{2.5}$$

Change in the entropy is calculated with Equation (2.6):

$$\varphi = \varphi_2 - \varphi_1 \tag{2.6}$$

The gas constant, R, of the working fluid is found by Equation (2.7):

$$R = (287.05 - 0.00990 \cdot f + 10^{-7} \cdot f) \cdot 10^3 \tag{2.7}$$

The ratio of the specific heat capacities, γ, of the working fluid is calculated by using c_p and R, which were previously calculated. Equation (2.8) gives the specific heat capacity ratio.

$$\gamma = {c_p}\Big/{(c_p - R)} \tag{2.8}$$

For more accurate calculations in each section, reduced pressure [26], P_r, shall be determined as in Equation (2.9):

$$P_r = exp\left({(\varphi - \varphi_0)}\Big/{R}\right) \tag{2.9}$$

In Equation (2.9), φ_0 is equal to 4.810138 $kJ/kg \cdot K$. Under the isentropic assumption, the change in temperature corresponds to the change in pressure which is related to the reduced pressure.

While performing design-point calculations, the Newton-Raphson method is used to calculate the temperature for some stations where the temperature is unknown. The temperature that matches the enthalpy is found iteratively for these engine stations by making an initial guess.

After the determination of these previously mentioned properties, the speed of sound of the working fluid can be calculated by using Equation (2.10).

$$a = \sqrt{\gamma RT} \tag{2.10}$$

By introducing the air model mentioned until this point, calculations for the turboshaft engine stations can be initiated.

2.3 Design Point Calculations

Calculations for stations are started by determining the freestream properties by using altitude, km (kilometers), and temperature deviation from ISA, ΔT (Kelvins) [12].

$$T_0 = 288.15 - 6.5 \cdot km + \Delta T \tag{2.11}$$

$$P_0 = 101.325\left(1 - \left(6.5 \cdot {km}/{288.15}\right)^{5.2558}\right) \tag{2.12}$$

For the sake of consistency, total pressure and temperature ratios between the inlet and exit of each station through the engine are defined in Equations (2.13) and (2.14).

$$\pi = {(P_{total})_{exit}}/{(P_{total})_{inlet}} \tag{2.13}$$

$$\tau = {(h_{total})_{exit}}/{(h_{total})_{inlet}} \tag{2.14}$$

For turboshaft engine design, the exhaust pressure ratio also is an essential factor that compares the exhaust nozzle exit total pressure with the freestream static pressure and calculated with Equation (2.15).

$$\pi_e = {(P_{total})_8}/{P_0} \tag{2.15}$$

According to engine requirements and design solutions, this value changes between 1.02 and 1.04, as stated by Erk [25].

Mass flows for individual stations are calculated with Equations (2.16) to (2.20):

$$\dot{m}_0 = \dot{m}_{1\rightarrow 2} = \dot{m}_{2\rightarrow 3} \tag{2.16}$$

$$\dot{m}_{3.1} = \dot{m}_0(1 - \beta_{Customer} - \beta_{Cooling1} - \beta_{Cooling2}) \tag{2.17}$$

$$\dot{m}_4 = \dot{m}_0\left(1 - \beta_{Customer} - \beta_{Cooling1} - \beta_{Cooling2}\right) \cdot (1 + f) \tag{2.18}$$

$$\dot{m}_{4.1} = \dot{m}_0 \left(\left(1 - \beta_{Customer} - \beta_{Cooling1} - \beta_{Cooling2}\right) \cdot (1 + f) + \beta_{Cooling1}\right) \tag{2.19}$$

$$\dot{m}_{4.5} = \dot{m}_0 \left(\left(1 - \beta_{Customer} - \beta_{Cooling1} - \beta_{Cooling2}\right) \cdot (1 + f) + \beta_{Cooling1} + \beta_{Cooling2}\right) \tag{2.20}$$

In the above equations, β represents the bleed taken from the compressor section, and subscripts represent the purpose of a taken bleed. Cooling flows are sometimes necessary to increase the engine life and operation capability. Since turbines are the sections that encounter the highest temperature flow, cooling flows reduce the temperature of this incoming flow to operate turbines more efficiently.

The usage of bleed air is optional in the code. The bleed extraction options are divided into two:

- The specified amount of air
- Percent of the core flow

After determining the mass flows for different stations, another important parameter, f, can be defined as the ratio of the supplied fuel to a combustion chamber and airflow at the inlet of the combustion chamber; it is calculated with Equation (2.21).

$$f = {\dot{m}_{fuel}}\Big/{\dot{m}_{3.1}} \tag{2.21}$$

Defining the mass flows also leads to establishing the corrected flow rate (see Equation (2.22)) term. This term can be explained as an amount of mass that would flow through a component if the inlet pressure and the temperature are equal to International Standard Atmosphere (ISA) conditions at sea level (e.g., 101.325 kPa, 288.15 K), which is another essential parameter for the design.

$$\dot{m}_{corr} = \dot{m}\left(\sqrt{\frac{T_{total}}{288.15}}\Big/\frac{P_{total}}{101.325}\right) \tag{2.22}$$

In addition, component stagnation pressure ratios are calculated in terms of reduced pressures and polytropic efficiencies to achieve higher accuracy, as in Equations (2.23) to (2.25).

$$\pi_C = \left({P_{r3}}/{P_{r2}}\right)^{\eta_{\infty c}} \tag{2.23}$$

$$\pi_{GGT} = \left({P_{r4.4}}/{P_{r4.1}}\right)^{1/\eta_{\infty ggt}} \tag{2.24}$$

$$\pi_{PT} = \left({P_{r5}}/{P_{r4.5}}\right)^{1/\eta_{\infty pt}} \tag{2.25}$$

Equation (2.26) is used for the combustion chamber calculations, which satisfies the energy balance at the inlet and exit.

$$(1+f)\left(h_{total4} - h_{ref}\right) + \left(h_{total3} - h_{ref}\right) = f \cdot \eta_{burner} \cdot LHV \tag{2.26}$$

Subscript “ref” represents the condition where the sea level ISA conditions are considered.

The energy balance between the compressor and the gas generator turbine is calculated using Equation (2.27).

$$\dot{m}_2(h_{total3} - h_{total2}) + {P_{ext}}/{\eta_{ext_{shaft}}} = \dot{m}_{4.1}(h_{total4.1} - h_{total4.4})\eta_{con} \quad (2.27)$$

In the above equation, $\eta_{ext_{shaft}}$ is the power extraction shaft efficiency and η_{con} is the efficiency of the spool that is connecting the compressor and the gas generator turbine. From Equation (2.27), the enthalpy of the gas generator turbine, $h_{total4.4}$, is found. Then, using the Newton-Raphson method, the temperature is found from the enthalpy. After calculating temperature, the turbine's reduced pressure and pressure ratio are calculated, respectively. These calculations also lead to the determination of power turbine inlet conditions.

For the power turbine section, calculating the pressure ratio depends on the pressure ratios of all components. The corresponding equation for the power turbine pressure ratio is given in Equation (2.28):

$$\pi_{pt} = \pi_C \cdot \pi_{ggt} \cdot \pi_{ram} \cdot \pi_{diffuser} \cdot \pi_{burner} \cdot \pi_{nozzle} \cdot \pi_{Cooling1} \cdot \pi_{Cooling2} \cdot {1}/{\pi_e} \quad (2.28)$$

Then, the Mach number at the inlet of the nozzle (exit of the power turbine section) can be calculated by manipulating Equation (2.29).

$${P_5}/{P_{ambient}} = \left(1 + {(\gamma_8 - 1)}/{2}\, M^2\right)^{{\gamma_8}/{\gamma_8 - 1}} \quad (2.29)$$

The static temperature is calculated using the Mach number, as in Equation (2.30).

$$T_{static} = {T_{total}}\Big/{1 + {(\gamma_8 - 1)}/{2} \cdot M^2} \quad (2.30)$$

After calculating the static temperature, velocity is calculated with Equation (2.31).

$$V = M \cdot \sqrt{\gamma_8 R\, T_{static}} \quad (2.31)$$

Since the mass flows are already calculated in the previous steps, the required area for a particular mass flow rate is obtained by using Equation (2.32).

$$A_8 = \frac{\dot{m}}{P_{ambient} / R\, T_{static}\, V} \tag{2.32}$$

2.4 Design Point Module Results and Comparison with GasTurb 14

A design point analysis module is created by combining the equations and approaches described up to this point. Several simulations with different engine design parameters and flight conditions were conducted to ensure the reliability of the design point module. After observing consistent results through the simulations, it is decided to use the inputs given in Table 2-4.

Table 2-4 Input Parameters of the Design Point Module

➢ Pressure Altitude	1500	m
➢ Ambient Temperature (It is optional to use ISA+ selection)	ISA+0	K
➢ Aerodynamic Interface Plane Mach Number	0.2	
➢ Corrected Air Flow at Inlet	3.5	kg/s
➢ Power Extraction	0	kW
➢ Bleed Air Percentage	0	
➢ Cooling Flow 1 Percentage	0	
➢ Cooling Flow 2 Percentage	0	
➢ Inlet Pressure Ratio	0.99	
➢ Freestream Pressure Recovery	0.99	
➢ Compressor Polytropic Efficiency	0.82	
➢ Compressor Pressure Ratio (Design choice)	13	
➢ Combustion Chamber Efficiency	1	
➢ Pressure Loss Through Combustion Chamber	4	%
➢ Lower Heating Value	43124	MJ/kg
➢ Combustion Chamber Exit Temperature (Limiting design parameter)	1450	K
➢ Gas Generator Turbine Polytropic Efficiency	0.85	
➢ Power Turbine Polytropic Efficiency	0.87	
➢ Exhaust Pressure Ratio	1.03	
➢ Power Extraction Shaft Efficiency	1	
➢ Gas Generator Shaft Efficiency	0.99	

➢ Power Turbine Shaft Efficiency	0.98	

The reason behind introducing the inputs different from ISA conditions at sea level is to control the corrections on mass flow rates, temperatures at different engine stations, and rotational speeds of the compressor and turbine. As a result of these input sets, outputs given in Figure 2-2 are achieved.

Station	mflow(kg/s)	T(K)	P(kPa)	m_corr(kg/s)
Ambient(0)		278.4005	84.5571	
1	3.0130	280.6331	86.9501	
2	3.0130	280.6331	86.0806	3.5000
3	3.0130	674.5165	1.1190e+03	0.4174
3.1	3.0130	674.5165	1.1190e+03	
4	3.0796	1450	1.0743e+03	0.6516
4.1	3.0796	1450	1.0743e+03	0.6516
4.4	3.0796	1.1287e+03	303.1914	
4.5	3.0796	1.1287e+03	303.1914	2.0370
5	3.0796	867.2192	87.0938	6.2155
8	3.0796	867.2192	87.0938	

PWSD (kW)	952.5964
SFC (kg/kWh)	0.2540
Fuel Flow (kg/s)	0.0672
A8 (m2)	0.0743

Component	Poly. Eff.	Isent. Eff.	Press. Ratio
Compr.	0.8200	0.7503	13
Burner	1		0.9915
HPT	0.8500	0.8681	3.5433
LPT	0.8700	0.8865	3.4812

Figure 2-2 Design Point Results of the Developed Code

GasTurb 14 results with the same inputs are given in Figure 2-3.

```
          W         T         P       WRstd
Station  kg/s        K        kPa      kg/s       PWSD     =     952.6 kW
 amb               278.40    84.556
  1      3.013     280.63    86.948               PSFC     =   0.25409 kg/(kW*h)
  2      3.013     280.63    86.078     3.500     Heat Rate=  10957.6 kJ/(kW*h)
  3      3.013     674.03  1119.018     0.417     V0       =     66.90 m/s
 31      3.013     674.03  1119.018               FN res   =      0.17 kN
  4      3.080    1450.00  1074.258     0.652     WF       =   0.06723 kg/s
 41      3.080    1450.00  1074.258     0.652     Therm Eff=  0.32854
 43      3.080    1128.38   303.195               P2/P1    =   0.99000
 44      3.080    1128.38   303.195               TRQ      =     100.0 %
 45      3.080    1128.38   303.195     2.037     P45/P44  =   1.00000
 49      3.080     866.16    87.093               Incidence=  0.00000 °
  5      3.080     866.16    87.093     6.213     P6/P5    =   1.00000
  6      3.080     866.16    87.093
  8      3.080     866.16    87.093     6.213     P8/Pamb  =   1.03000
Bleed    0.000     674.03  1119.016               WBld/W2  =   0.00000
-------------------------------------------       A8       =   0.07430 m²
Efficiencies:   isentr  polytr    RNI    P/P      WCHN/W2  =   0.00000
 Compressor     0.7504  0.8200  0.877 13.000      WCHR/W2  =   0.00000
 Burner         1.0000                0.960      Loading  =    100.00 %
 HP Turbine     0.8683  0.8500  1.604  3.543      WCLN/W2  =   0.00000
 LP Turbine     0.8867  0.8700  0.603  3.481      WCLR/W2  =   0.00000
 Generator      1.0000                           PW_gen   =     952.6 kW
-------------------------------------------
HP Spool mech Eff 1.0000  Nom Spd  38000 rpm
PT Spool mech Eff 1.0000  Nom Spd  10000 rpm     eta t-s  =   0.86923
-------------------------------------------
hum [%]     war0       FHV      Fuel
   0.0   0.00000    43.124    Generic
```

Figure 2-3 Design Point Results of the GasTurb 14

As it may be concluded from the outputs given in Figure 2-2 and Figure 2-3, shaft powers delivered (PWSD) and specific fuel consumptions (SFC) are almost the same. These two parameters are considered since the main aim is to provide high power with minimum SFC. In addition, mass flows and pressures differ at a maximum rate of 0.13% and 0.0013%, respectively. So, it can be concluded that the results are highly compatible with the reference software.

2.4.1 Parametric Design Point Study

To determine the design point, which is the most optimal point for the engine to be designed, many points in the operating envelope should be considered and compared. After achieving satisfactory results for a single point, a parametric design point study is initiated to optimize the cycle as suggested in [18]. When the comparisons are made considering the design parameters and limitations, a carpet plot of the engine parametric design is obtained, as seen in Figure 2-4.

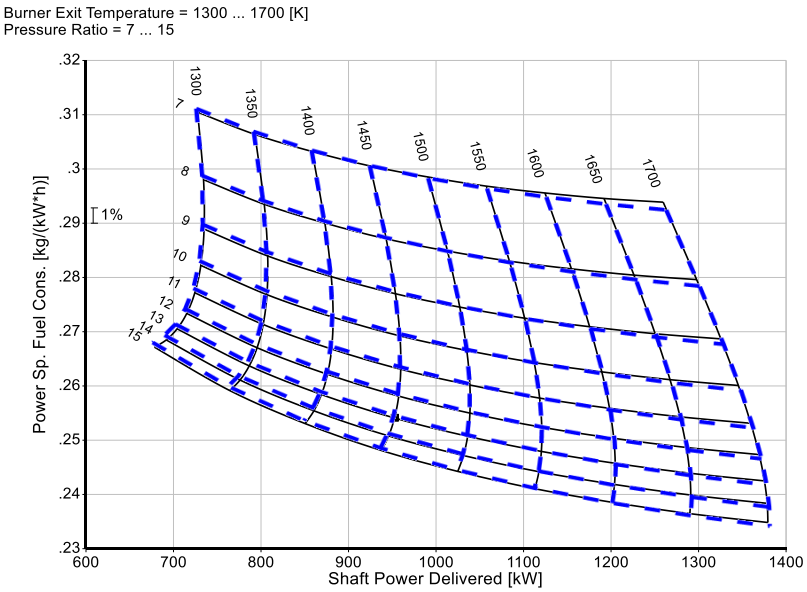

Figure 2-4 Parametric Design Point Study

As shown in Figure 2-4, both the compressor pressure ratio and the gas generator turbine input temperature change. The resultant shaft power outputs and SFCs are

plotted for each of these values. Results are again highly compatible with GasTurb 14 outputs (in the upper right corner, the SFC value of the developed code differs from the GasTurb at around 0.5%, where the maximum error is observed). In Figure 2-4, the blue line represents the developed code results while the black line represents the GasTurb 14 results.

CHAPTER 3

OFF-DESIGN PERFORMANCE CALCULATIONS

The next step for engine design and performance calculations in line with the chosen limitations and design parameters is off-design calculations. After completing engine design point cycle calculations, the performance of the specific engine is determined for varying compressor-gas generator shaft rotational speeds. So, performing the off-design calculations leads to establishing the engine performance for all the steady-state operational behavior. For this purpose, generic maps of the components are scaled according to the outputs of the design point analysis.

The following sections briefly describe the map scaling and calculation process to accomplish the off-design calculations.

3.1 Map Scaling Procedure

As previously discussed, component characteristics are mainly determined by the design point calculations. For this reason, the compressor and turbine maps should be scaled using the design point analysis results. The initial step for scaling the component maps is to convert the graphical maps into tables. Performing such an operation requires a digitization tool. In this study, Engauge software was used for this purpose.

Due to the shape of speed lines in the compressor map, reading the performance parameters may lead to incorrect results (See Figure 3-1; “?” marks indicate that there may be more than one pressure ratio for the same mass flow rate and vice versa because the speed lines are almost horizontal for relatively low speeds and almost vertical for high speeds.). The Beta-Line Technique is used to prevent this, as suggested by Walsh and Fletcher [12]. Beta lines are parallel and equally spaced

arbitrary lines, ranging from 0 to 1. The surge line is also one of the beta lines, and its beta value is 1. In the developed code, there are 20 beta lines located in the compressor map. The representative shape of the beta lines in the compressor map is illustrated in Figure 3-1.

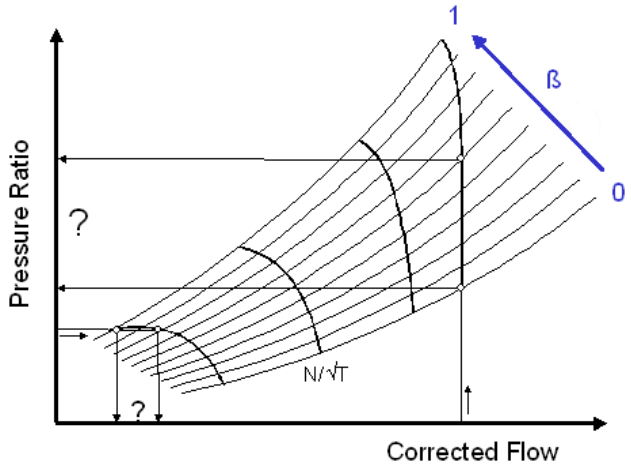

Figure 3-1 Compressor Map Beta Lines [16]

After implementing the beta lines to the compressor map, the tabulated form of the performance parameters are presented in Figure 3-2.

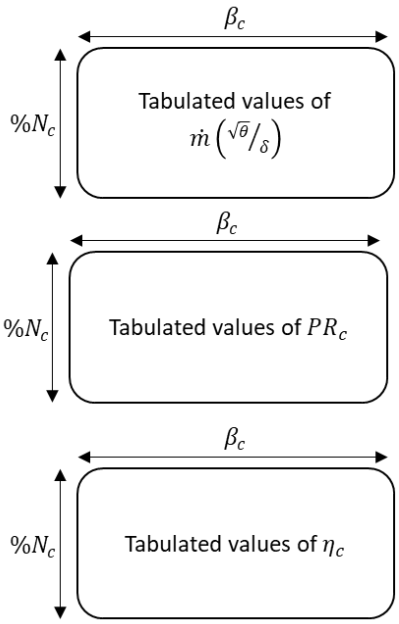

Figure 3-2 Tabulated Compressor Map Structure

Once the look-up tables are constructed, performance parameters which are corrected mass flow rate, pressure ratio, and isentropic efficiency scaled with Equations (3.1) to (3.3), as suggested by Kurzke et al. [17]:

$$PR = \frac{PR_{des} - 1}{PR_{map,des} - 1}\left(PR_{map} - 1\right) + 1 \tag{3.1}$$

$$\dot{m}\sqrt{\theta}/_{\delta} = \frac{\left(\dot{m}\sqrt{\theta}/_{\delta}\right)_{des}}{\left(\dot{m}\sqrt{\theta}/_{\delta}\right)_{map,des}}\left(\dot{m}\sqrt{\theta}/_{\delta}\right)_{map} \tag{3.2}$$

$$\eta_{isen} = \frac{\eta_{isen,des}}{\eta_{isen,map,des}}\,\eta_{isen,map} \tag{3.3}$$

Where subscript "des" represents the design point value of the related parameter, "map, des" represents the design point value of the reference map and "map" represents the scaling point in the reference map.

Applying the scaling procedure to the compressor map, all the necessary data to calculate the required parameters at the compressor exit is achievable for the specific compressor-gas generator spool speed and beta line.

At this point, since the compressor map table contains the performance parameters concerning corrected speed, the compressor-gas generator turbine and power turbine spool speed shall be considered in terms of corrected speed as given in Equation (3.4).

$$\%N_c = \frac{N_{ggt}/\sqrt{\theta}}{\left(N_{ggt}/\sqrt{\theta}\right)_{des}} \tag{3.4}$$

A similar procedure could also be applied to the turbine maps by considering the beta lines parallel to the x-axis.

Reference maps for the related components are listed as follows:

- NASA TM 101433 for compressor map,
- NASA TM83655 for gas generator turbine map, and
- AGARD two-stage turbine map for power turbine map as suggested in [16].

3.2 Steady-State Component Matching Procedure in Off-Design

The operating points of the engine for the specified conditions are unique and determined by applying the thermodynamic matching procedure. Previously constructed map tables include all the required information for matching the components. They are iteratively read and matched using Newton-Raphson Algorithm as described by Kurzke et al. [17]. Thus, steady-state operating line generation by matching the components is an iterative process.

Four iteration variables are accounted for as independent variables. These variables are:

1. β of the compressor,
2. Gas generator turbine inlet temperature,
3. β of the gas generator turbine,
4. β of the power turbine.

Based on these iteration variables, four inter-connected errors appear for each iteration and are tried to be minimized for converging results. These errors are also suggested by Kurzke et al. [17] and listed as follows:

1. Flow compatibility between combustion chamber and gas generator turbine
2. Work compatibility between compressor and gas generator turbine
3. Flow compatibility between gas generator turbine and power turbine
4. Difference between required and actual pressure at the nozzle section

In the developed code, the iteration continues until the square of the sum of the errors is less than 10^{-8}. When the convergence condition is satisfied, the iteration variables are uniquely found for a specific input condition.

The representative flowchart of the method is given in Figure 3-3.

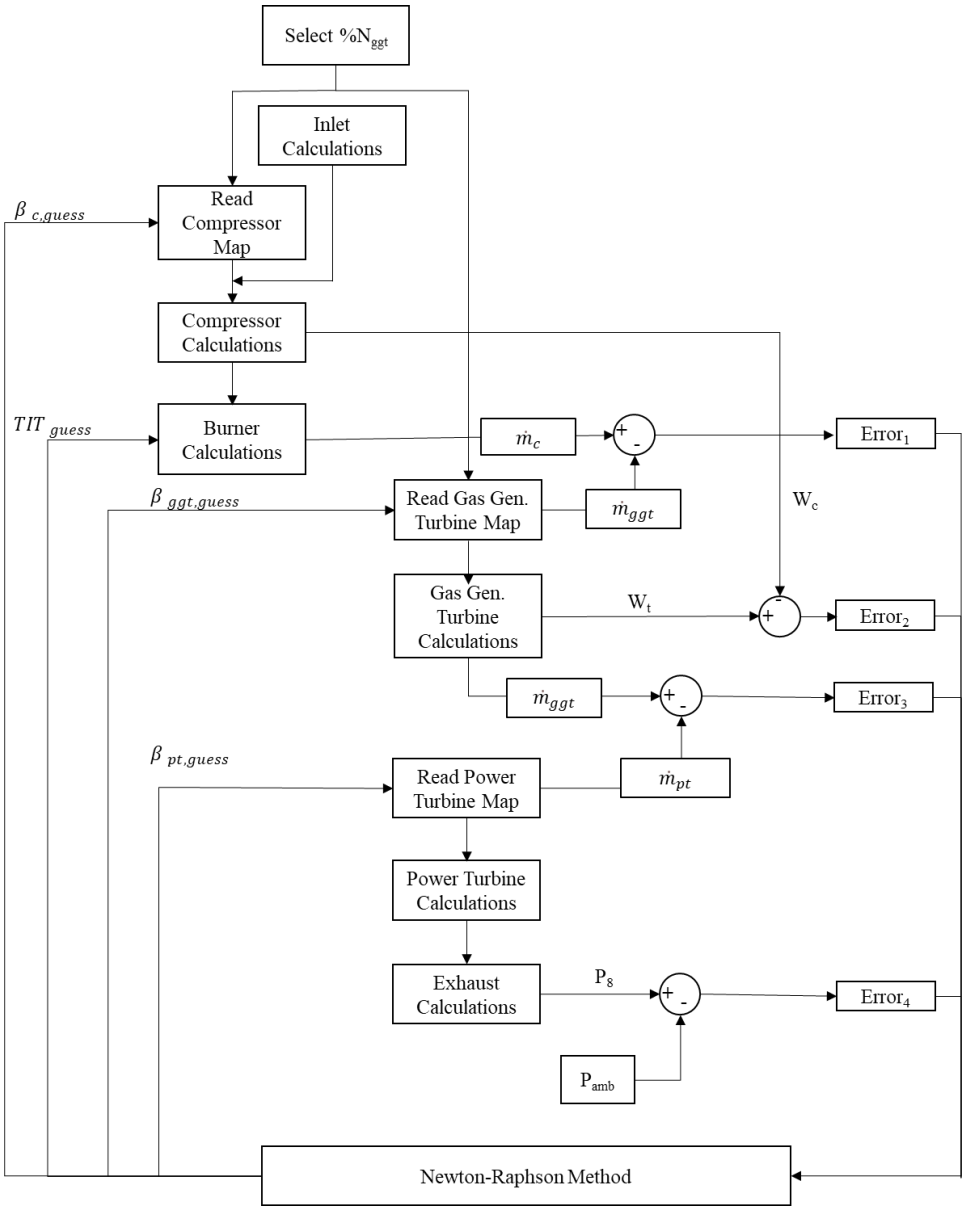

Figure 3-3 Off-Design Matching Algorithm

3.3 Off-Design Module Results and Comparison with GasTurb 14

The operating line can be achieved by applying the above procedure with desired spool speeds, as shown in Figure 3-4. For ease of comparison with the GasTurb results, calculated operating points are presented in the same compressor map generated by the developed code.

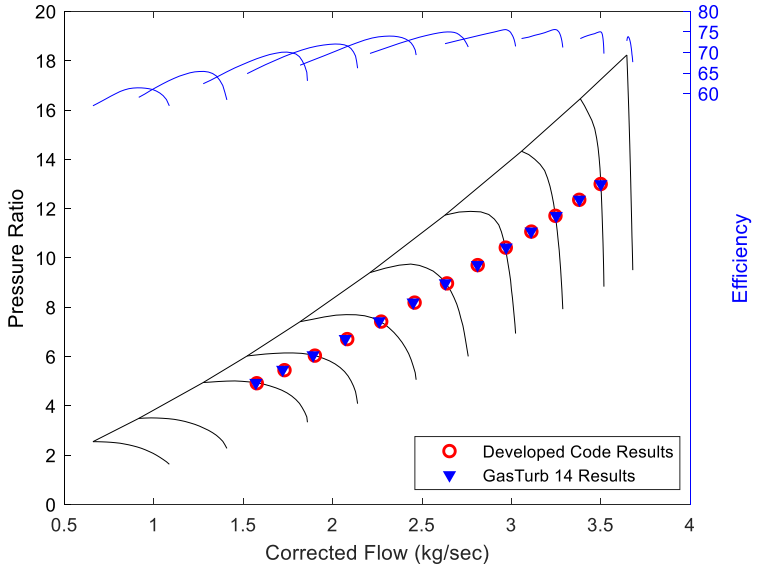

Figure 3-4 Off-Design Steady-State Operating Line

In Table 3-1 and Table 3-2, GasTurb 14 results and developed code results are tabulated for a detailed comparison.

Table 3-1 Comparison of the Results with GasTurb 14 - 1

Relative Speed	**Developed Code**			**GasTurb 14**			**Absolute % Diff**		
	$\dot{m}_{corr}$	PR_c	T_4	$\dot{m}_{corr}$	PR_c	T_4	$\dot{m}_{c,corr}$	PR_c	T_4
0.7	1.575	4.92	1060.3	1.568	4.94	1064.37	0.44	0.49	0.39
0.725	1.730	5.45	1075.5	1.722	5.47	1078.94	0.44	0.29	0.32
0.75	1.900	6.04	1095.4	1.891	6.06	1098.19	0.49	0.33	0.26
0.775	2.081	6.71	1122.3	2.072	6.72	1124.46	0.42	0.22	0.20
0.8	2.271	7.42	1153.4	2.259	7.44	1156.42	0.52	0.30	0.26
0.825	2.458	8.19	1192.0	2.449	8.2	1195.10	0.37	0.18	0.26
0.85	2.639	8.97	1231.2	2.633	8.98	1236.13	0.23	0.17	0.40

Relative Speed	Developed Code			GasTurb 14			Absolute % Diff		
	$\dot{m}_{corr}$	PR_c	T_4	$\dot{m}_{corr}$	PR_c	T_4	$\dot{m}_{c,corr}$	PR_c	T_4
0.875	2.811	9.71	1270.7	2.805	9.72	1274.38	0.20	0.15	0.29
0.9	2.968	10.42	1306.1	2.966	10.43	1308.86	0.06	0.10	0.21
0.925	3.111	11.07	1338.7	3.110	11.08	1340.62	0.01	0.05	0.14
0.95	3.246	11.71	1371.4	3.245	11.71	1373.82	0.02	0.04	0.18
0.975	3.379	12.36	1407.3	3.380	12.37	1409.56	0.04	0.08	0.16
1	3.500	13.00	1450.0	3.500	13	1449.99	0.00	0.00	0.00
Mean							**0.25**	**0.19**	**0.24**

Table 3-2 Comparison of the Results with GasTurb 14 - 2

Relative Speed	Output Power (kW)		
	Developed Code	**GasTurb 14**	**Absolute % Diff**
0.7	104.47	103.73	0.71
0.725	142.61	141.89	0.50
0.75	187.88	188.97	0.58
0.775	245.65	248.07	0.99
0.8	312.88	315.54	0.85
0.825	388.77	391.61	0.73
0.85	473.02	475.24	0.47
0.875	556.61	559.34	0.49
0.9	635.57	639.75	0.66
0.925	711.90	715.40	0.49
0.95	788.11	791.51	0.43
0.975	868.25	871.95	0.43
1	952.60	952.55	0.00
Mean			**0.56**

As it may be concluded from Table 3-1 and Table 3-2, both results are compared in terms of compressor corrected flow, compressor pressure ratio, gas generator turbine inlet temperature, and power outputs. Since the maximum error is observed as 0.99% for the power output, the developed code is compatible with GasTurb 14 in terms of off-design steady-state performance calculations. The differences between code and GasTurb can be caused by the different sets of equations used to develop the air model and solve for the components (e.g., reduced pressure terms in given Equations (2.23) to (2.25) are not defined in GasTurb).

CHAPTER 4

TRANSIENT PERFORMANCE CALCULATIONS

The next step in designing an engine and performance analysis code is determining the engine's transient behavior. In transient operations, there is a time-dependent change in performance parameters and this dependency on time differs transient operations from steady operations. Transient behavior is observed mainly for the following regimes:

1. Start-up,
2. Emergency Cases,
3. Acceleration and Deceleration (Load Changes),
4. Relight.

During these regimes, the state of an engine varies between steady-state thermal equilibrium points. As a result of thermal and mechanical stresses from state changes, engine health and reliability are affected. Therefore, the transient behavior of the engine needs to be analysed with high accuracy.

What is common in all transient regimes is the effect of polar moment of inertia on the behavior of the engine response. Especially the rotating components' inertias should be taken into consideration. Before going into details of the transient analysis, it is apparent that there is more fuel demand to achieve the desired operating condition during engine acceleration than the steady operation. For decelerating maneuvers, the situation is vice versa.

Due to the turboshafts' working principle, which maintains the constant power turbine speed in general, an unbalanced power (UPW) term is added to the work compatibility between the compressor and gas generator turbine, as described by Walsh and Fletcher [12]. The sign of UPW is positive for the accelerating maneuvers since the fuel flow is increased, and this increase causes a mismatch between

compressor and gas generator turbine. In this scenario, due to the addition of extra fuel, the power of the gas generator turbine is greater than the compressor and auxiliary powers if there is any. On the contrary, gas generator turbine work does not match the compressor and auxiliary works due to a lack of fuel flow during deceleration. So that turbine work is inadequate to operate the compressor. Because of that, the UPW sign is negative for decelerating operations. A modified version of the work compatibility (Equation (2.27)) is used to accomplish these operations by adding a term UPW, as given in Equation (4.1).

$$UPW + \dot{m}_2(h_{total3} - h_{total2}) + \frac{P_{ext}}{\eta_{ext_{shaft}}} = \dot{m}_{4.1}(h_{total4.1} - h_{total4.4})\eta_{con} \tag{4.1}$$

Unlike the steady-state analysis, fuel flow is introduced as an input for the transient performance calculations. Thanks to the Newton-Raphson algorithm, UPW is predicted according to the desired fuel flow at each iteration and is tried to be minimized. In other words, one should notice that UPW is always zero for the steady-state operation. For this reason, when the analysis converges for the transient regime, rate of 10^{-11} UPW is considered a satisfactory convergence error.

This matching procedure is applied for each time step defined by the user; as soon as the convergence is satisfied for the current step, then the code starts to calculate related parameters for a step further.

Spool acceleration/deceleration rate is calculated with Equation (4.2):

$$dN/dt = UPW/I\,N\left(\frac{2\pi}{60}\right)^2 \tag{4.2}$$

Then, Euler Integration Method is applied to obtain the rotational speed of the spool in the next time step as:

$$N_{t+1} = N_t + dN/dt\,\delta t \tag{4.3}$$

The process for matching the components in the transient regime is briefly explained in Figure 4-1.

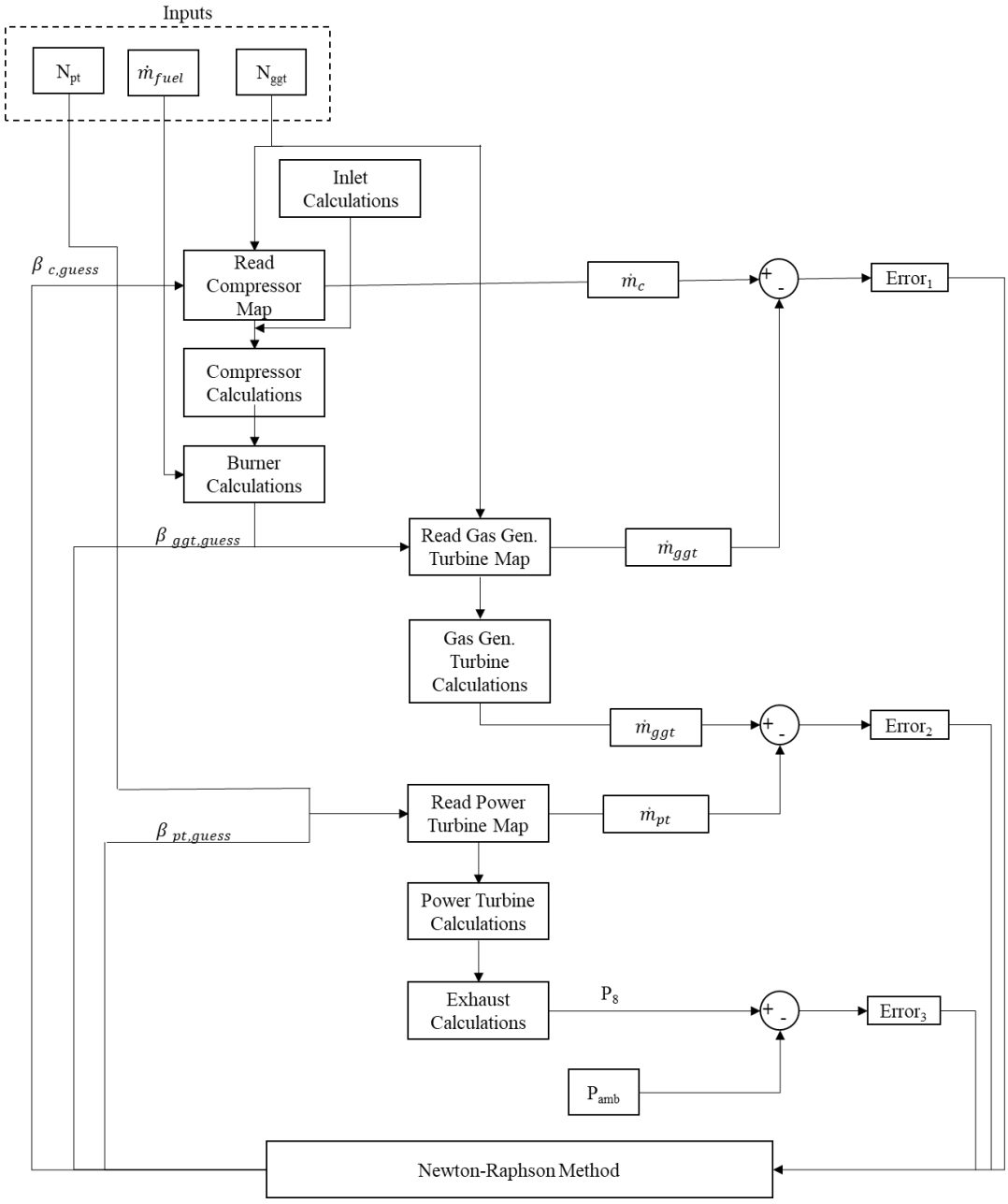

Figure 4-1 Transient Component Matching Algorithm

The procedure given in Figure 4-1 with the Euler integration method to determine the inputs at each time step is given in Figure 4-2.

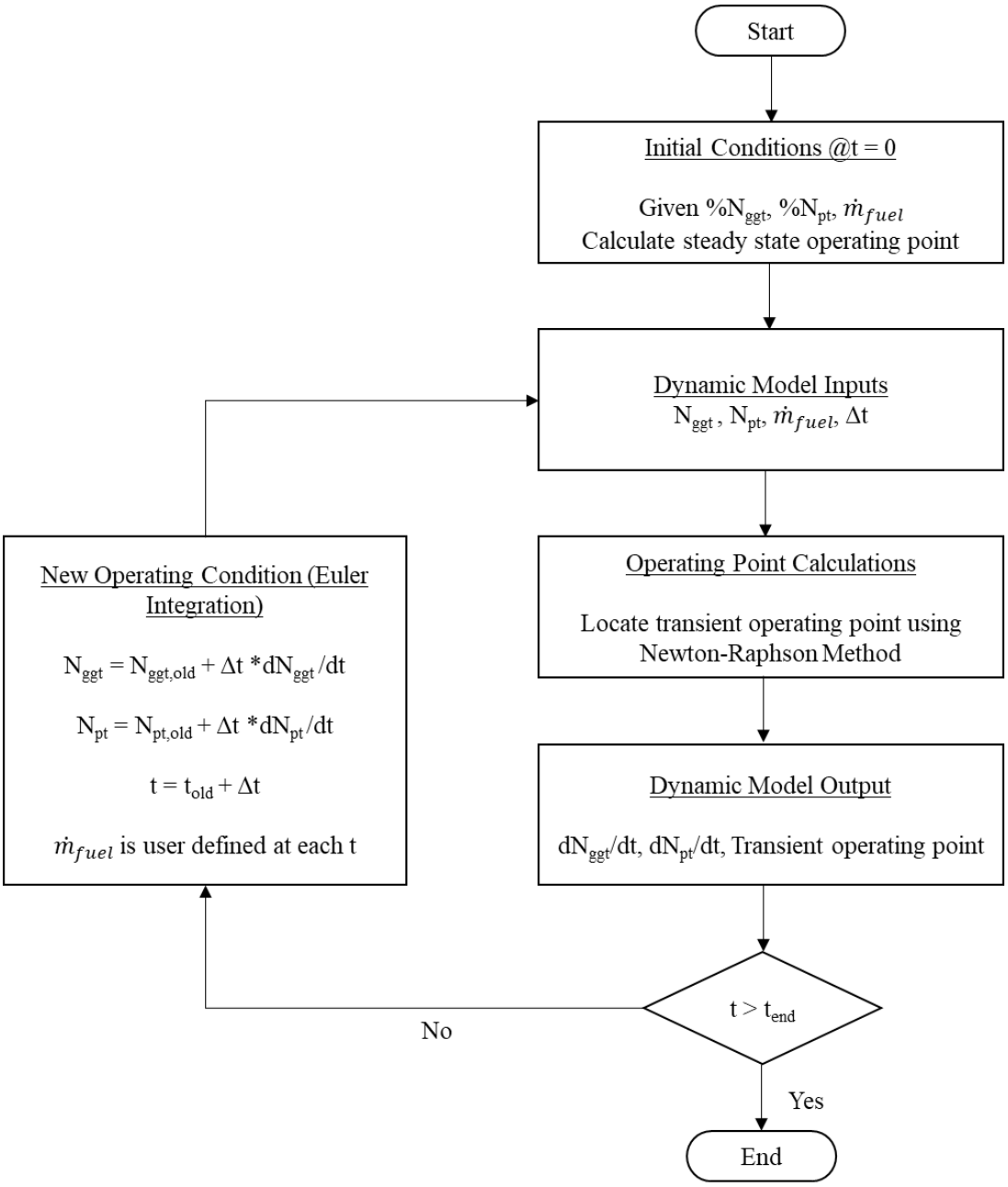

Figure 4-2 Transient Performance Calculation Algorithm

As the rate of change of spool speed approaches zero, the convergence is satisfied for the developed code.

4.1 Transient Module Results and Comparison with GasTurb 14

Since off-design steady-state results are in close agreement with GasTurb 14, step fuel inputs are introduced, which are calculated for each steady-state operating point. Gas generator turbine spool speed and gas generator turbine inlet temperature behaviors are observed in response to the fuel inputs. Values for the applied flow rates are given in Table 4-1.

Table 4-1 Applied Fuel Flow Rates

Steps (%Ng Variations)	$\dot{m}_{fuel}$***(kg/sec)***
Step 1 (0.7 - 0.725)	0.021
Step 2 (0.725 - 0.75)	0.024
Step 3 (0.75 - 0.775)	0.027
Step 4 (0.775 - 0.8)	0.031
Step 5 (0.8 - 0.825)	0.035
Step 6 (0.825 - 0.85)	0.040
Step 7 (0.85 - 0.875)	0.045
Step 8 (0.875 - 0.9)	0.050
Step 9 (0.9 - 0.925)	0.055
Step 10 (0.925 - 0.95)	0.059
Step 11 (0.95 - 0.975)	0.064
Step 12 (0.975 - 1)	0.070

Figure 4-3 contains the fuel flow step inputs and gas generator turbine spool speed in response to the fuel inputs.

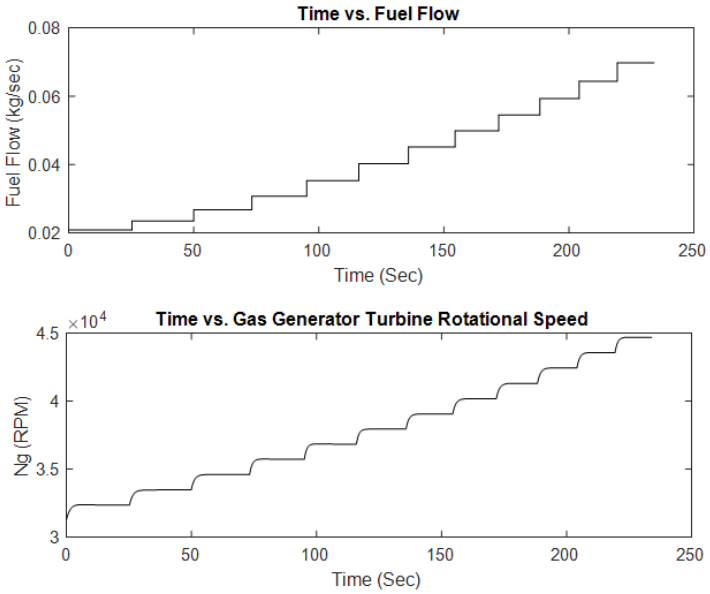

Figure 4-3 Fuel Flow Rate Step Inputs and Response of Gas Generator Turbine

In Figure 4-3, all the states run for off-design analysis are presented, and it is concluded that as the convergence is achieved, the results are the same as the steady-state. In order to observe the behavior of the engine more clearly, the gas generator turbine inlet temperature and gas generator turbine rotational speed at which the engine reaches the design point is shown in Figure 4-4. For the sake of verification of the results, outputs are given with the GasTurb 14 outputs.

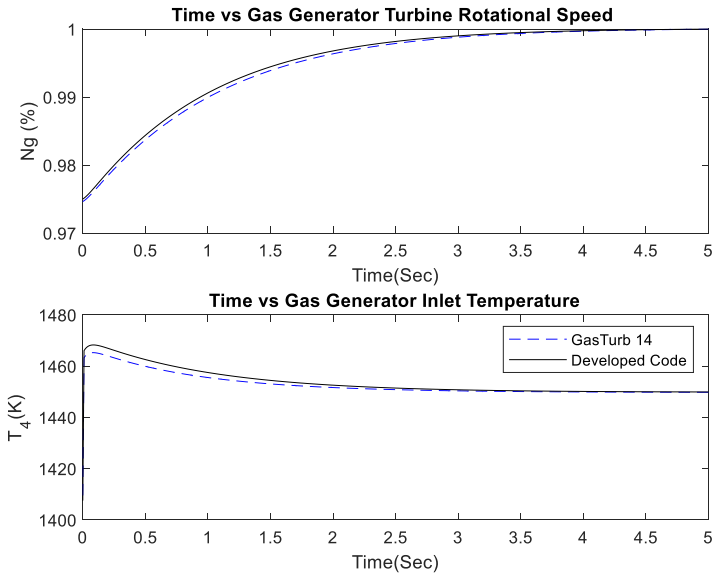

Figure 4-4 Time vs Ng and T_4

In Figure 4-4, it can be seen that convergent results are compatible as expected. Although the temperature peak value is higher and the acceleration schedule is faster than the GasTurb 14 results, both outputs are quite similar. This difference can also be caused by the use of different sets of equations used to develop the air model and solve for the components, as mentioned in Chapter 3.3. In addition, the difference can also be caused by fuel pump modeling in GasTurb, as stated by Erk [25].

CHAPTER 5

VALIDATION OF THE DEVELOPED CODE

5.1 GE T700 Engine Model Description

In addition to comparing the results with GasTurb 14 outputs, the performance modeling of the developed code is compared with the GE T700 engine, which is widely used in the literature for validation purposes. While modeling the engine, station numbering, which is given in Figure 5-1 is used.

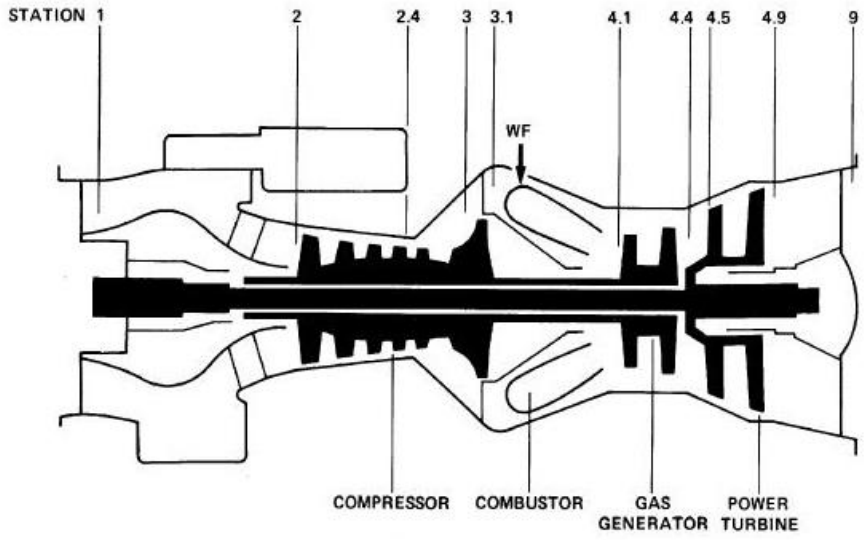

Figure 5-1 T700 Engine Station Numbering [27]

Ambient conditions are considered ISA at sea level, as given in Uzol's study [28]. It is assumed that there are no inlet losses, such that compressor inlet conditions are the same as the ambient conditions. Throughout the analysis of the T700 engine, the compressor map given in Figure 5-2 is used as suggested by Ballin et al. [27] and Uzol [28]. In Uzol's study [28], compressor map is constructed by using multi-layer neural network.

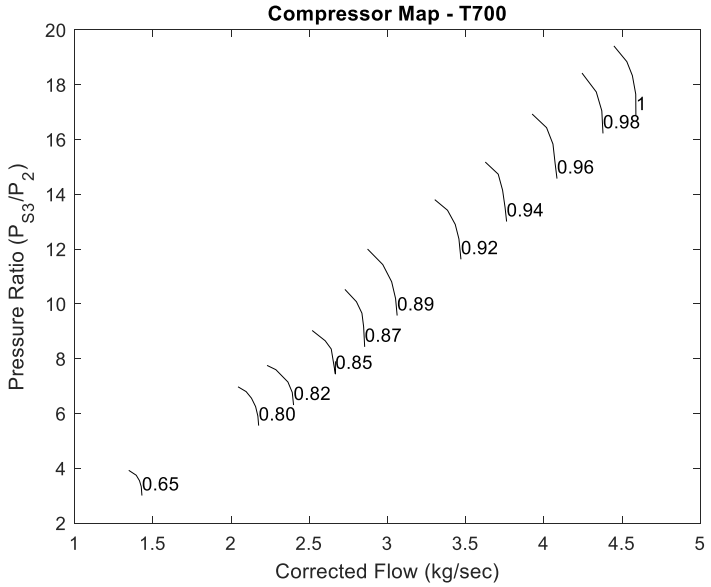

Figure 5-2 Compressor Pressure Ratio and Mass Flow Relation - GE T700

It should be noted that compressor corrected flow equals the compressor inlet flow thanks to the assumptions of ISA conditions and no inlet losses.

In Figure 5-2, the efficiency information of the compressor is not included in the performance map. Instead, the pressure and temperature ratio of the compressor is given in Figure 5-3, as represented by Ballin et al. [27] and Uzol [28].

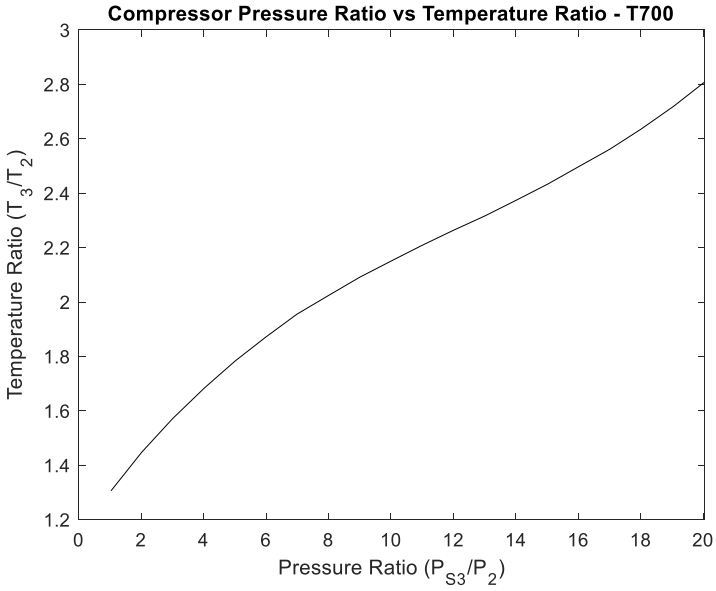

Figure 5-3 Compressor Pressure Ratio and Temperature Ratio Relation

The relationship between the temperature and pressure ratios of the compressor leads to the calculation of efficiencies by using Equation (5.1):

$$\eta_c = \frac{\pi_c^{(\gamma-1)/\gamma} - 1}{\tau_c - 1} \tag{5.1}$$

In the reference engine model, there are three bleed fractions from the compressor section, and their non-linear relations are given in Appendix A through Figure A-1 to Figure A-3. These extracted bleeds are used for different purposes and are described in [27].

For the calculations of the combustion chamber, the combustion chamber efficiency is taken as 98.5% as depicted in [27], and does not vary with the f.

According to Mihaloew et al. [29] and Szuch et al. [30], the performance of the gas generator turbine is handled by considering both the enthalpy drop parameter and the corrected mass flow rate. According to Glassman et al. [31], critical velocity is required for the enthalpy drop parameter to be determined only by the pressure ratio. Since there is no gas generator turbine map in the reference papers, the component

is modeled by considering the relation between pressure ratio and enthalpy drop parameter (see Figure A-4). At this point, it should be noted that if one needs to determine mass flow through the gas generator turbine, the engine is considered to operate at its nozzle in a choked flow condition over the operating envelope. This procedure allows the calculation of mass flow rate and corrected mass flow rate.

By using the relation given in Figure A-4, the enthalpy value at the gas generator turbine exit can be calculated from the pressure ratio, enthalpy drop parameter, and critical speed at the inlet of the gas generator turbine.

Similar to the calculation procedure for the gas generator turbine, the determination of the critical speed for the power turbine is necessary for the calculations. Enthalpy change through the power turbine is then calculated using the same approach as the gas generator turbine. The relation between the enthalpy drop parameter and power turbine pressure ratio is given in Figure A-5.

Once the enthalpy drop is calculated, enthalpy and temperature at the power turbine outlet can also be determined. The corrected flow rate of the power turbine is then determined by the relation given in Figure A-6.

One last relation is used to calculate the exhaust pressure ratio. In the reference Ballin's study [27], the curve that relates exhaust pressure ratio and gas generator turbine speed is given in Figure A-7.

All the relations are digitized throughout the modeling process, and an appropriate curve fitting method is applied. In addition, the explicitly created constants for the reference GE T700 engine are used and can be found in Ballin's study [27] with Imperial Units and Novikov' s study [32] with Metric Units.

As a result of implementing the model into the developed code, engine steady and transient performances are simulated; the results with details are described in the following.

Initially, parameters given in Table 5-1 are set for the design point inputs:

Table 5-1 GE T700 Input Parameters

π_c	17.5	
$\dot{m}_{inlet}$	4.57	kg/sec
$T_{4.1}$	1520	K
γ_{loss}	0.988	
N_{ggt}	44700	rpm
N_{pt}	20900	rpm
J_{ggt}	0.06033	Nms^2
J_{pt}	0.08406	Nms^2

For steady-state simulations, the method applied to accomplish transient analysis is used as described in Chapter 4, and fuel flow inputs are introduced from 0.019 kg/s to 0.107 kg/s as suggested by Ballin [27] (as discussed in the previous chapter, when the convergence is satisfied, results are the same with the steady-state ones). Results of the steady-state analysis are shown in Figure 5-1.

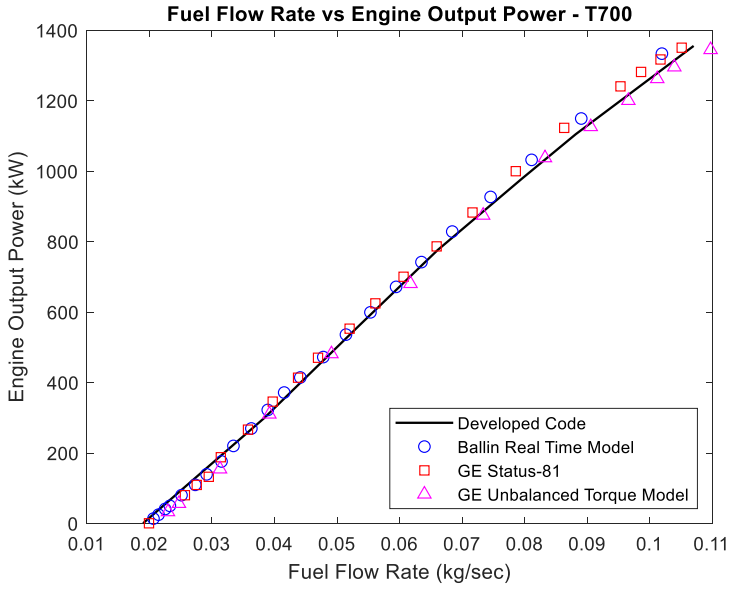

Figure 5-4 Steady-State Results Comparison with the Published Data

In the reference paper, Ballin's real-time model is developed and compared with the NASA Lewis simulation, which is validated with the experimental engine. As can be observed from Figure 5-4, the results are compatible with the literature data. The difference between the model and literature data can be caused by the table

digitization or assumptions of compressor pressure ratio and temperature at the gas generator turbine inlet, which are given in Table 5-1.

Ballin's study [27] is also considered for the transient performance simulation results. The reference paper considers heat soakage and volume dynamics approximations while modeling. In the developed code, heat soakage effect is not considered. Therefore, heat transfer effects between engine metal parts and working fluids are not implemented. During the transient performance simulation of the GE T700 engine, fuel flow suddenly increased from 0.0504 kg/sec to 0.0976 kg/sec. As a result of this step input of the fuel flow, engine acceleration response is observed by considering gas generator turbine speed with turbine inlet temperatures as given in Figure 5-5.

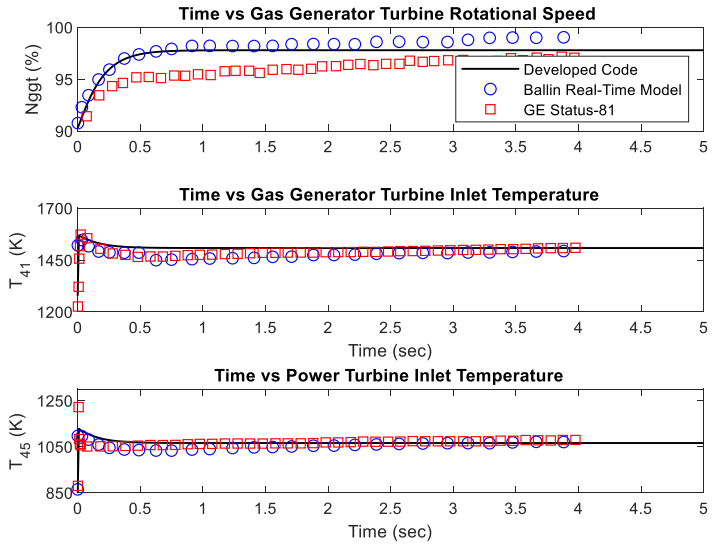

Figure 5-5 Transient Simulation Results of GE T700 Engine

Figure 5-5 shows that the results become more consistent over time, although some differences exist between the literature data and the developed model. The initial assumptions in Table 5-1 can be cited as the reason for these differences, especially for the initial and converged values. In addition, due to the lack of detailed turbine maps, some numerical deviations may occur between the results of the code and the data given in the literature.

The different characteristics observed during the transient, heat soakage model, and volume dynamics approaches can be the reasons. The heat soakage model affects the engine's behavior during transients and delays the convergence of each parameter due to the heat transfer effects.

CHAPTER 6

COMPRESSOR MAP GENERATION AND FOULING EFFECTS ON PERFORMANCE

Determining the engine's steady-state and transient performance with the developed code depends on the component maps. These detailed maps contain information on the corrected mass flow rate, overall pressure ratio, corrected rotational speed, and isentropic efficiency of each component. In this respect, these tables' importance in calculating the components' performance cannot be disregarded.

As it can be understood from what has been explained so far, a compressor is one of the main elements that make up the gas turbine, and therefore it greatly impacts the overall performance. However, for most cases, performance -compressor map- data are not publicly available, and all these data depend on the individual stage performance of a multistage compressor. In those cases, the stage-stacking method is used to construct an overall performance map of the compressor.

6.1 Stage-Stacking Method

In the stage-stacking method, individual stage performances are calculated, and results are combined to evaluate the overall performance. For the application of this method, the following non-dimensional parameters are needed to be determined for each stage:

- Flow coefficient

$$\phi = {}^{C_x}/_{u} \tag{6.1}$$

- Pressure rise coefficient

$$\psi = c_p T_{0_{stage}} \frac{PR^{(\gamma-1/\gamma)} - 1}{u^2} \tag{6.2}$$

- Temperature rise coefficient

$$\zeta = c_p \frac{\Delta T_{0_{stage}}}{u^2} \tag{6.3}$$

- Efficiency

$$\eta = \frac{T_{0_{stage}} PR^{(\gamma-1/\gamma)} - 1}{\Delta T_{0_{stage}}} = \psi/\zeta \tag{6.4}$$

In order to model each stage, the following generalized non-dimensional parameters are also needed to be determined as given in Equation (6.5).

$$\psi^* = \frac{\psi}{\psi_{ref}}, \phi^* = \frac{\phi}{\phi_{ref}}, \eta^* = \frac{\eta}{\eta_{ref}} \tag{6.5}$$

In Equation (6.5), the selection of reference points is significant for calculating stage characteristics. A running line can be used to determine the reference values, which means that the highest efficiency points lie on the running line of the compressor.

Based on this approach, the curve in Figure 6-1 ($\psi^* = f_\psi(\phi^*)$) is obtained by the results of many experiments and relates ψ^* and ϕ^*, as depicted in the study of Muir et al. [33].

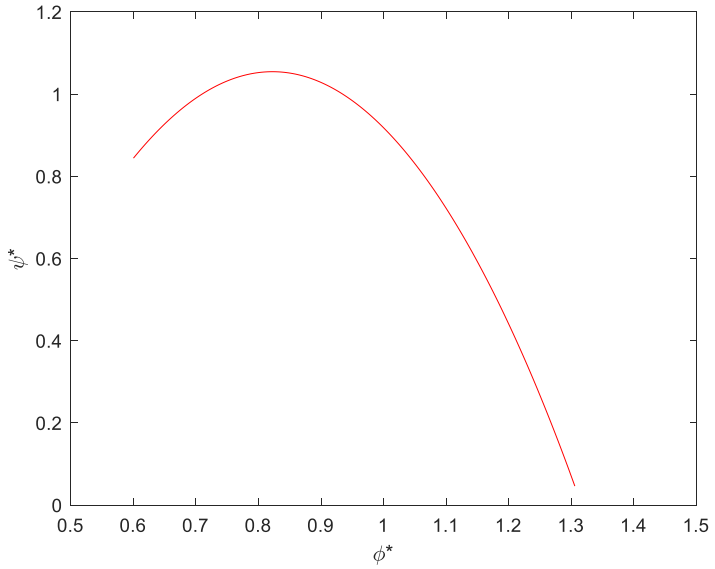

Figure 6-1 Generalized Stage Pressure Coefficient Curve

Then, this curve is approximated by Equation (6.6):

$$\psi^* = \frac{\psi}{\psi_{ref}} = \psi^*_{max} - \frac{\psi^*_{max} - 1}{\left(\phi^*_{\psi^*_{max}} - 1\right)^2} \left(\phi^*_{\psi^*_{max}} - \phi^*\right)^2 \tag{6.6}$$

The generalized efficiency relationship is acquired from the curve in Figure 6-2, which Howell and Bonham [34] suggest.

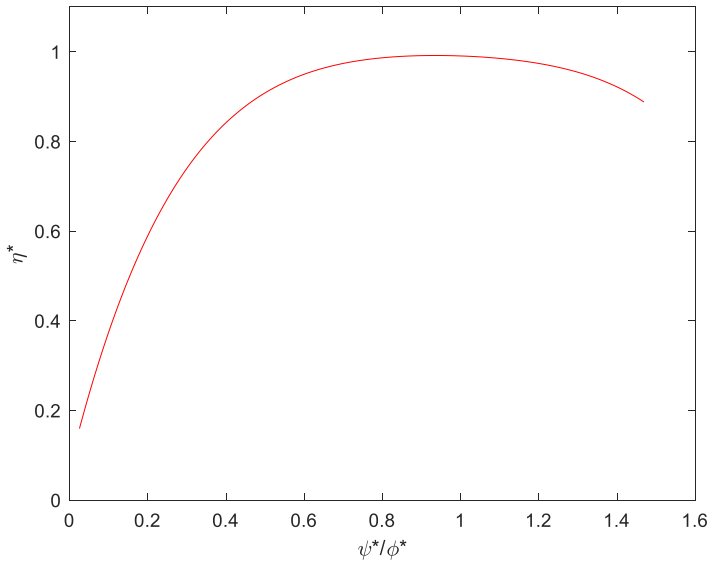

Figure 6-2 Generalized Stage Efficiency Curve

This relationship, $\eta^* = f_\eta\left(\frac{\psi^*}{\phi^*}\right)$ is derived from the curve in Figure 6-2 by implementing the Equations (6.7) and (6.8):

$$\eta_1^* = \frac{\eta}{\eta_{ref}} = 1 - \frac{1 - \eta^*_{\left(\frac{\psi}{\phi}\right)min}}{\left(1 - \left(\frac{\psi^*}{\phi^*}\right)_{min}\right)^{3.5}} \left(1 - \frac{\psi^*}{\phi^*}\right)^{3.5}, where\ \frac{\psi^*}{\phi^*} < 1 \qquad (6.7)$$

$$\eta_2^* = \frac{\eta}{\eta_{ref}} = 1 - \frac{1 - \eta^*_{\left(\frac{\psi}{\phi}\right)max}}{\left(\left(\frac{\psi^*}{\phi^*}\right)_{max} - 1\right)^2} \left(\frac{\psi^*}{\phi^*} - 1\right)^2 \ where\ \frac{\psi^*}{\phi^*} > 1 \qquad (6.8)$$

These generalized non-dimensional parameters are acquired to ease the modeling process.

After determining the characteristics of individual stage performance, compressor inlet parameters such as inlet flow, total inlet pressure, total inlet temperature, and corrected compressor speed are stated to initiate the stage-stacking procedure.

6.2 GE LM2500-30 Compressor Map Generation by Using Stage-Stacking Method

GE LM2500-30 engine is one of the most popular reference engines for the study of compressor map generation and deterioration, thanks to available literature data about flow field and operating conditions. The engine is a two-spool turboshaft with sixteen stages axial compressor and variable guide vanes at the first six stages. The engine cutaway is given in Figure 6-3.

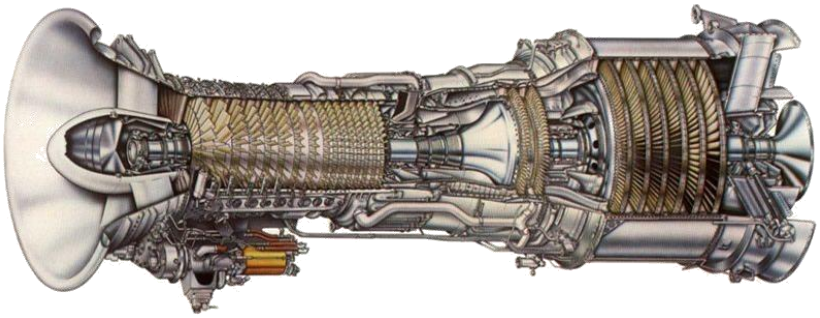

Figure 6-3 GE LM2500-30 Turboshaft Engine Cutaway [35]

Since the manufacturer does not publish the compressor map, the stage-stacking method is used to develop a compressor map of the engine. There are also other studies published by Muir et al. [33] and Mathioudakis et al. [36] on the reference engine, which apply the stage-stacking method to generate the overall compressor performance map.

In Chapter 6.1, it is mentioned that generalized curves are needed to determine the performance parameters, and these curves are usually generated by considering the highest efficiency reference points. Operating points on the running line of the reference engine correspond to these highest efficiency points. These running line data for the GE LM2500-30 compressor are tabulated in Table 6-1. These data are sufficient to establish reference non-dimensional parameters for the generalized curves mentioned in the previous section (see Figure 6-1 and Figure 6-2), as well as the reference values of the parameters.

Table 6-1 Running Line of the GE LM2500-30 Compressor [33]

$\mathbf{N/\sqrt{\theta}}$	**PR**	$\mathbf{(\dot{m}\sqrt{\theta})/\delta}$	$\mathbf{\Delta T/T}$
9450	18.06	66.90	1.530
9160	17.21	65.31	1.439
8971	16.25	62.51	1.389
8813	15.30	59.69	1.343
8660	14.37	56.93	1.307
8508	13.44	54.07	1.262
8364	12.45	50.89	1.220
8105	10.35	43.86	1.112
7772	7.88	34.75	0.983

Data in Table 6-1 provide shaft speed, mass flow rate, pressure ratio, and efficiency of the complete compressor section. However, these data should be converted to non-dimensional parameters for the stage characteristics determination. Conversion of these data requires the velocity diagrams at the inlet of the rotor (primarily axial flow velocity and blade speed). By applying the conservation of mass relation to each stage, velocities at the axial direction can be calculated as given in Equation (6.9):

$$\dot{m} = \rho \cdot C_x \cdot A \tag{6.9}$$

Here, C_x is the axial flow velocity.

In the above equation, static density is used and cannot be determined without knowing the absolute velocity at the inlet of the rotor. If absolute flow angle at rotor inlet (α_1) is a known parameter, Equation (6.10) can be used to find absolute flow velocity:

$$C_1 = C_x \,/\, cos\,(\alpha_1) \tag{6.10}$$

Rotor inlet absolute flow angle varies commensurately with the acting rod position for stator blades with varying geometry. This rod position also varies with shaft speed. Reference engine compressor, rod angle, and absolute flow angle at the inlet of stages are publicly available data (shown in Figure 6-4).

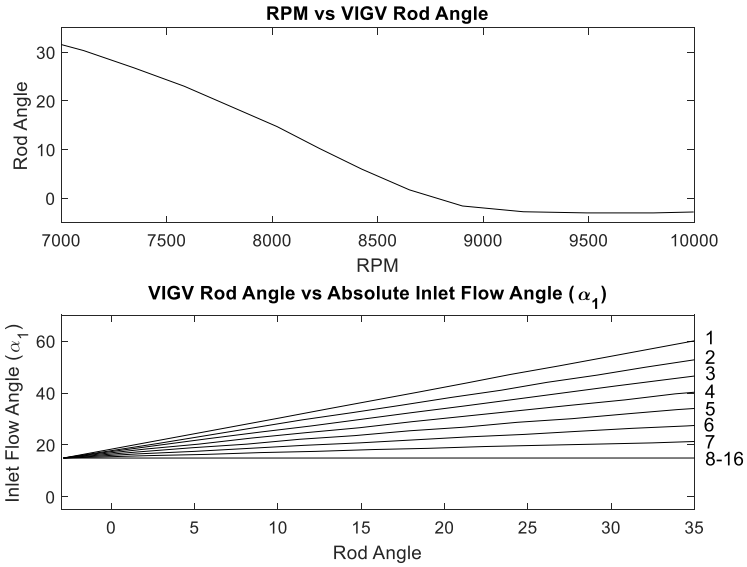

Figure 6-4 Acting-Rod Position and Stage Outlet Angle for A GE LM2500-30 Engine with VIGV and Six Variable Geometry Stages [33]

Velocity vectors with the absolute flow angle are demonstrated in Figure 6-5 for clarification.

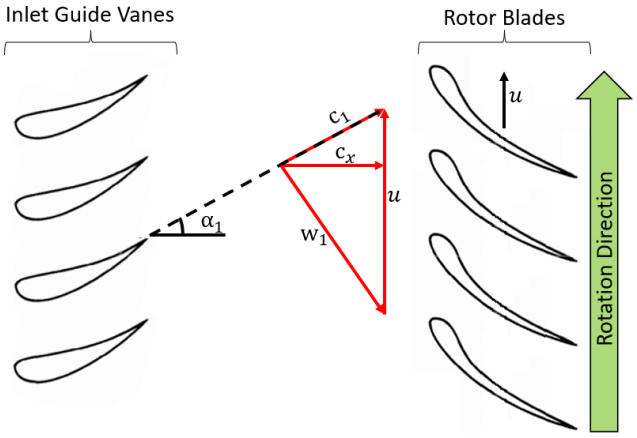

Figure 6-5 Velocity Diagram of Variable Guide Vanes and Rotor Blades

In addition to the axial velocity, blade tangential velocity is found by using Equation (6.11).

$$u = \omega \cdot r \tag{6.11}$$

The required geometrical data to apply this procedure is given in Table 6-2.

Table 6-2 Gas Path Geometry of GE LM2500-30 Compressor Model [33]

Stage	$\bar{r}$**[m]**	$A[m^2]$	**Stage**	$\bar{r}$**[m]**	$A[m^2]$
1	0.2794	0.3568	9	0.3112	0.1374
2	0.2835	0.3310	10	0.3122	0.1213
3	0.2819	0.3039	11	0.3129	0.1058
4	0.2913	0.2761	12	0.3139	0.0929
5	0.2954	0.2471	13	0.3147	0.0819
6	0.2992	0.2181	14	0.3157	0.0723
7	0.3033	0.1877	15	0.3165	0.0652
8	0.3071	0.1561	16	0.3175	0.0581

At this point, it should be noted that determining the stage performance parameters is an iterative process. In detail, each compressor stage impacts the performance of the other stages. Calculations are performed starting from the first stage until the last stage, and iterations are done with this sequence. While making calculations, the output conditions of the leading stage are considered the inlet conditions of the next stage. In other words, it is assumed that there is no loss through the stator vanes; this is why there are no stator vanes in Figure 6-5. Also, it is assumed that all the stages have the same isentropic work, which means the temperature change and efficiencies of all the stages are identical.

During the modeling process, the operating conditions are assumed to be ISA at sea level without any inlet loss, which allows for determining the compressor's inlet pressure and temperature. Thus, iterations to search for stage performance parameter values are initiated with the combination of thermodynamic properties (i.e., axial velocity and total density are used for the first iteration rather than static density). As noted, isentropic flow through the stages is assumed, and thanks to this assumption, Equations (6.12) and (6.13) are used to obtain the static density, pressure, and temperature.

$$\frac{T}{T_{total}} = \left(1 + \frac{\gamma - 1}{2} \cdot M^2\right)^{-1} \tag{6.12}$$

$$\frac{\rho}{\rho_{total}} = \left(1 + \frac{\gamma - 1}{2} \cdot M^2\right)^{-\frac{1}{\gamma - 1}} \tag{6.13}$$

As can be seen, all thermodynamic properties depend on the Mach number, and the Mach number depends on the static temperature value. In the calculation model, both Mach number and density are considered as dependent variables, and iteration is continued until the sum of the differences with the values found in the previous iteration becomes smaller than 10^{-5}. While generating a compressor map, reference values are found by considering the running line. Then the procedure is extended by introducing the mass flows for each rotational speed which are given in Table 6-1. By using the introduced mass flows and effective annulus areas, C_x is determined. This leads to the calculation of flow coefficients, ϕ, and ϕ^*. At this point, generalized flow, ϕ^*, and pressure rise coefficients, ψ^*, given in Equation (6.6) are used and ψ^* is calculated. Then, the procedure is followed by determining the remaining stage coefficient, which is efficiency. To accomplish this step of the calculation, generalized efficiency, η^*, relationships given in Equation (6.7) and Equation (6.8) are used with previously determined stage coefficients. Once the η is calculated, the temperature rise coefficient, ζ, is found with the relation given in Equation (6.4). Finding ζ allows determining the stage temperature rise and stage pressure rise accordingly. For the sake of clarity, the method is described with a flowchart in Appendix B.

Throughout the calculations, the following values that are provided by Spina [38] are used:

- $\psi^*_{max} = 1.115$
- $\phi^*_{\psi^*_{max}} = 0.835$
- $\eta^*_{\left(\frac{\psi}{\phi}\right)min} = 0.200$
- $\left(\frac{\psi^*}{\phi^*}\right)_{min} = 0.040$
- $\eta^*_{\left(\frac{\psi}{\phi}\right)max} = 0.920$
- $\left(\frac{\psi^*}{\phi^*}\right)_{min} = 1.460$

A compressor map is developed using the methodology described up to this point. However, there are minor differences between the pressure ratios of the developed

map and the map found in studies of Yang et al. [37] and Rodríguez et al. [41]. When the pressure ratio correction is applied to the developed compressor map, it becomes compatible with the map found in the references. Since [37] and [41] contain the same map, it is decided to be used as a reference compressor map for the fouling analysis of GE LM2500-30 engine. So, the compressor map in the reference papers is digitized with Engauge software, and the beta-line technique is applied. As a result of these operations, the compressor map shown in Figure 6-6 is found.

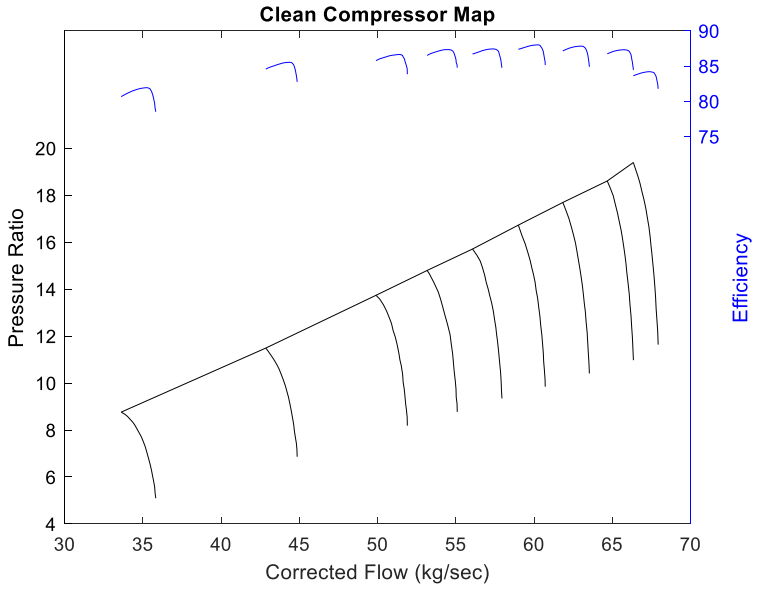

Figure 6-6 GE LM2500-30 Compressor Map

6.3 Performance Analysis of GE LM2500-30 with Clean Compressor

Compressor performance map determination from limited data and considering the fouling of that particular compressor is followed by the performance analysis. For this reason, developed code is used. As previously discussed, an engine design process originates from design point performance analysis followed by the generic component map scaling to determine detailed component maps. However, for the specific engine, which is GE LM2500-30, the compressor is developed by applying the stage-stacking method. It means that the compressor section's sizing, design limits, and performance parameters are already determined. Thanks to the data given

in Table 6-1, compressor design pressure ratio, temperature ratio, isentropic efficiency, and rotational speed at the design point are all available information.

Since it is known that the engine delivers 20 MW of output power at its design point, efficiencies of turbines and combustion chamber sections are assumed as follows. During the analysis, polytropic efficiencies are assumed as 90% and 80% for the gas generator turbine and power turbine, respectively. Combustion chamber efficiency is assumed as 98.5%. Considering the design point was set based on ISA conditions on sea level, the developed model provided 20 MW of output power as previously determined. Consequently, the design point results of the engine are satisfied.

6.3.1 Steady-State Off-Design Analysis of GE LM2500-30

After the completion of engine design point cycle calculations, the performance of the specific engine is determined by varying compressor-gas generator shaft rotational speed. So, performing the off-design calculations leads to establishing the engine performance for all the steady-state operation envelopes. The compressor and turbine maps are essential for these analyses. For this reason, two generic turbine maps are scaled according to the outputs of the design point analysis. The same method discussed in Chapter 3.1 is applied for the map scaling operations. The compressor map is not scaled since it is generated explicitly by the stage-stacking method.

Four iteration variables listed in Chapter 3.2 are used with the same errors. The algorithm (see Figure 3-3) for achieving the converged results is also the same. The running line is achieved for the specific speeds by applying the procedure with the desired spool speeds. The calculated results for the desired speeds are given in Figure 6-7.

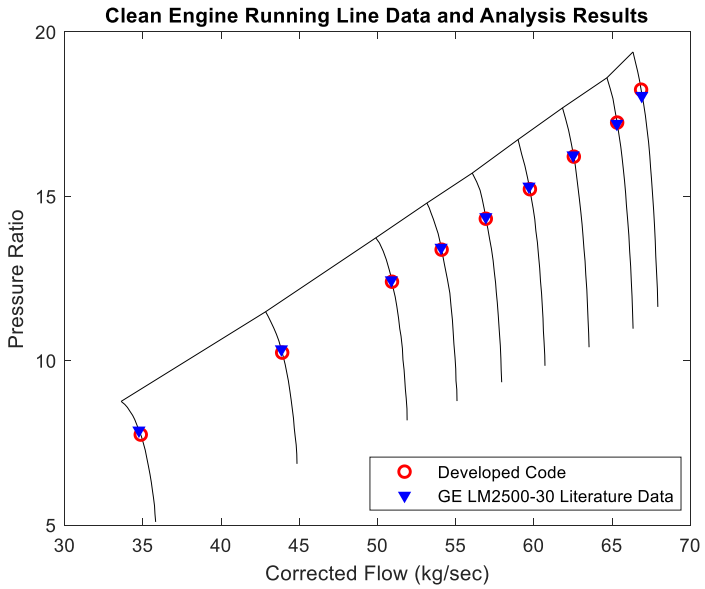

Figure 6-7 Off-Design Running Line of GE LM2500-30

As seen in Figure 6-7, converged results for each spool speed are compatible with the data points in the literature. Pressure ratios and mass flow rates are tabulated below for better comparison.

Table 6-3 Calculated Running Line Data vs Literature Data

$N/\sqrt{\theta}$	Calculated PR	Given PR (Table 6-1)	Error (%)	Calculated Corrected Flow	Given Corrected Flow (Table 6-1)	Error (%)
9450	18.25	18.06	-1.03	66.86	66.90	0.06
9160	17.25	17.21	-0.20	65.33	65.31	-0.03
8971	16.21	16.25	0.26	62.56	62.51	-0.07
8813	15.22	15.3	0.55	59.75	59.69	-0.10
8660	14.32	14.37	0.35	56.93	56.93	0.00
8508	13.38	13.44	0.46	54.10	54.07	-0.06
8364	12.40	12.45	0.38	50.93	50.89	-0.08
8105	10.25	10.35	1.00	43.91	43.86	-0.11
7772	7.75	7.88	1.63	34.87	34.75	-0.34

Since turbines are modeled from generic turbine maps, errors are mainly caused by the assumptions on turbine sections and combustion chamber. From Table 6-3, it can be seen that maximum error appears as 1.63%.

6.3.2 Transient Performance Analysis of GE LM2500-30

Performing satisfactory analyses of the particular engine in steady-state operating regimes is followed by considering the engine performance in transient regimes.

The same methodology as depicted in Chapter 4 is applied to the GE LM2500-30 engine. Therefore, fuel flows that are calculated in the steady-state analysis are required. Applied fuel flow rates are tabulated in Table 6-4.

Table 6-4 Applied Fuel Flow Rates – GE LM2500-30

$\mathbf{N/\sqrt{\theta}}$	$\dot{m}_{fuel}$*(kg/sec)*
9450	1.225
9160	1.077
8971	0.972
8813	0.877
8660	0.804
8508	0.722
8364	0.646
8105	0.482
7772	0.327

Since the steady-state values are compatible with the literature data, when the convergence is satisfied for each fuel input, the results are the same as the steady-state ones. Therefore, the behavior of the gas generator turbine with the applied fuel flow rates is represented in Figure 6-8.

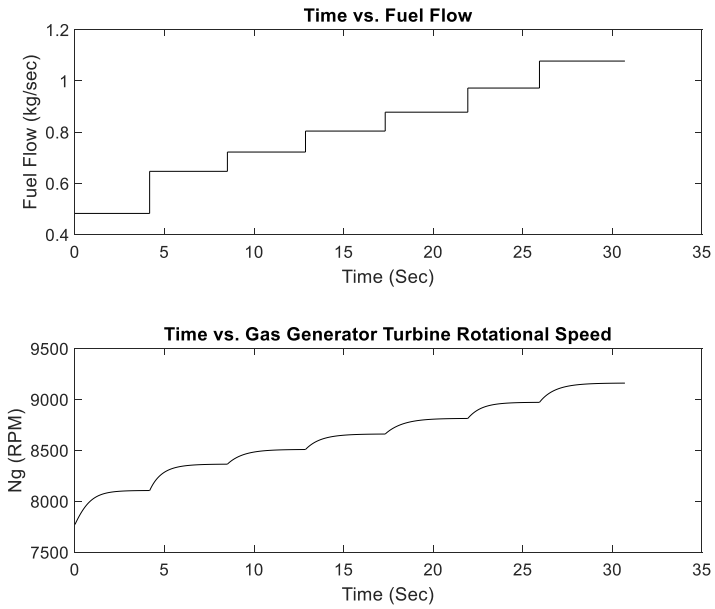

Figure 6-8 Fuel Flow and Gas Generator Turbine Spool Speed Transient Response

6.4 Deterioration Due to Fouling

The overall performance of the engine is highly dependent on environmental conditions. Due to environmental influences, the performance of gas turbines deteriorates. This deterioration is mainly caused by changes in the blade profiles of compressor and turbine sections. These changes on blade profiles are mainly due to:

- Fouling,
- Corrosion,
- Erosion,
- Foreign Object Damage (FOD).

Among these factors, it is estimated that the fouling on the compressor causes 70% to 85% of the performance losses of gas turbines according to Diakunchak [39]. Particles such as sand, dust, and salt could stick to the annulus and surface of the blades and cause changes in the profile. In addition to that, particles cause an increase in surface roughness. Fouled aerodynamic interface plane and axial compressor blades are represented in Figure 6-9. As a result of fouling, overall isentropic efficiency, inlet mass flow rate, and overall pressure ratio of the compressor degrades. Due to the degradation of these performance parameters, engine power output also degrades.

Figure 6-9 Fouled Compressor Inlet and Compressor Blades [40]

Many researchers are still studying the effects of fouling on compressors and overall gas turbines. In the publications of Yang et al. [37] and Rodríguez et al. [41], previous studies are presented in detail.

Research shows that fouling can reach 40% to 50% of the total compressor stages from the inlet, according to Aker and Saravanamuttoo [42]. Since the reference engine has 16 stages of the axial compressor, eight stages of it are assumed to be subjected to fouling for this study.

Investigation of the fouling effect on the compressor performance begins with determining the individual stage performances. For this purpose, fouling coefficients provided by Tarabrin et al. [43] are used. The coefficients relate the non-dimensional parameters and the operating time. These coefficients are determined from the curves given in Figure 6-10.

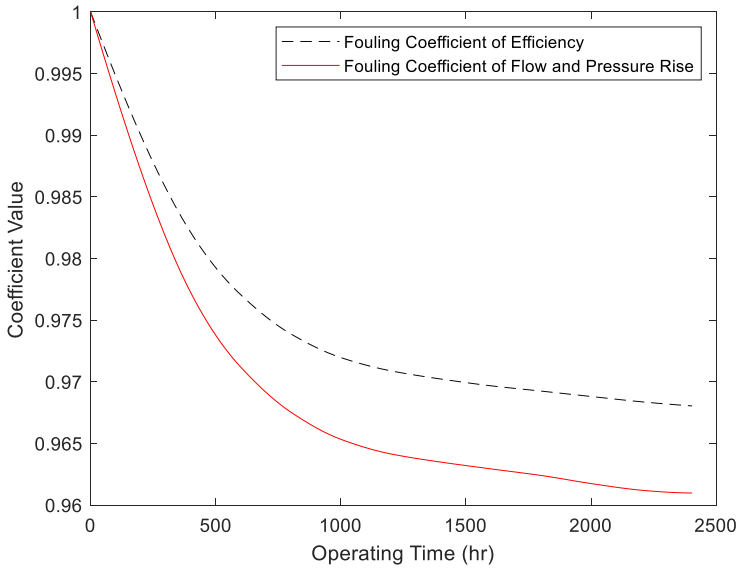

Figure 6-10 Fouling Coefficients

Thus, non-dimensional parameters with the effect of fouling are determined via Equations (6.14) to (6.16):

$$\phi_f = c_{\phi f} \cdot \phi_{ref} \tag{6.14}$$

$$\psi_f = c_{\psi f} \cdot \psi_{ref} \tag{6.15}$$

$$\eta_f = c_{\eta f} \cdot \eta_{ref} \tag{6.16}$$

Where $c_{\psi f}$, $c_{\phi f}$, and $c_{\eta f}$ are fouling coefficients that vary with the operating time. The smaller value of these coefficients means more severe fouling occurs in the stage.

Even for the same operating time, the performance parameters of the compressor may vary because fouling is not uniformly distributed along the stages. Because of that, severity factors should also be considered in addition to the time-dependent coefficient of fouling. These factors implicate the effects of physical properties of the ingested particles such as size, and material.

The first factor is considered by introducing the global fouling severity factor, FS_g, as suggested by MacIsaac [44]. According to MacIsaac, FS_g varies from 0 (clean engine) to 10 (deteriorated engine). After the determination of FS_g, relative severity factor, FS_i, is found for individual compressor stages using data given in Table 6-5. In Table 6-5, k_{FS_i} parameters are reordered from top to bottom as suggested in [41] since front stages are more susceptible to fouling. After the reordering process, data become compatible with Saravanamuttoo [42], [45] and Tarabrin et al. [46].

Table 6-5 Fault Severity Assignment Table

Stage Number	$\boldsymbol{k_{FS_i}}$
1	1.3
2	1.2
3	1
4	1
5	0.7
6	0.5
7	0.3
8	0.1

FS_i for individual stages are calculated with Equation (6.17).

$$FS_i = k_{FS_i} \cdot FS_g \tag{6.17}$$

Calculation of FS_i is then followed by modification of the reference conditions, which is very important for determining non-dimensional parameters and stage characteristics. In order to do this, fault severity factors for each non-dimensional parameter shall be identified, which is contained in Table 6-6 [37].

Table 6-6 Reference Point Modification Coefficients

FS	$\boldsymbol{k_{\phi,i}}$	$\boldsymbol{k_{\psi,i}}$	$\boldsymbol{k_{\eta,i}}$
0	1	1	1
1	0.96	0.99	0.95
2	0.92	0.98	0.9
3	0.88	0.97	0.85
4	0.84	0.96	0.8
5	0.8	0.95	0.75

FS	$k_{\phi,i}$	$k_{\psi,i}$	$k_{\eta,i}$
6	0.76	0.94	0.7
7	0.72	0.93	0.65
8	0.68	0.92	0.6
9	0.64	0.91	0.55
10	0.6	0.9	0.5

By considering data in Table 6-6, non-dimensional parameters with the modification of reference values are determined with Equations (6.18) to (6.20):

$$\phi_{f,i} = c_{\phi f} \cdot k_{\phi,i}(FS_i) \cdot \phi_{ref,i} \tag{6.18}$$

$$\psi_{f,i} = c_{\psi f} \cdot k_{\psi,i}(FS_i) \cdot \psi_{ref,i} \tag{6.19}$$

$$\eta_{f,i} = c_{\eta f} \cdot k_{\eta,i}(FS_i) \cdot \eta_{ref,i} \tag{6.20}$$

The method described so far is applied to the compressor section of the reference engine to simulate deterioration for 400 flight hours, and the resulting map is shown in Figure 6-11.

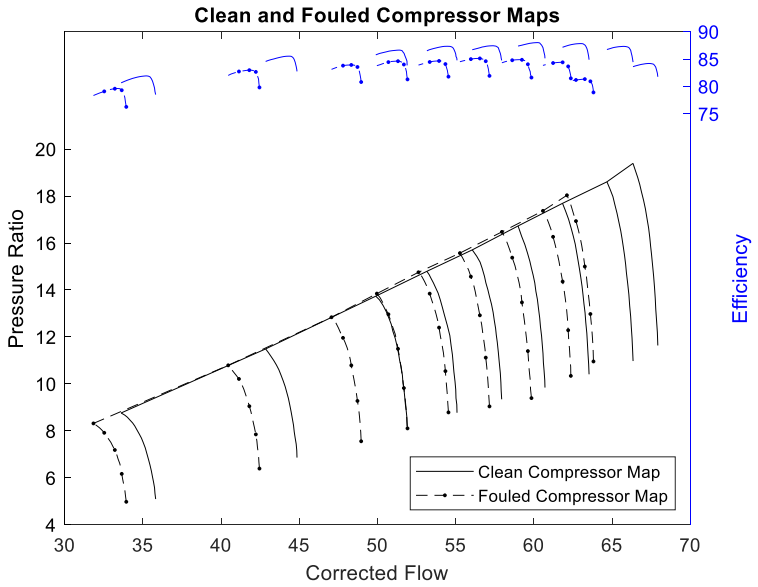

Figure 6-11 Clean and Fouled (400 Flight Hour) Compressor Map of GE LM2500-30 (with Modified MacIsaac Model with FS_g=1)

6.5 Fouling Effects on Engine Performance

After modeling the behavior of the clean engine in steady-state and transient maneuvers, the effect of fouling on performance will be examined in the following chapter. Since the design of the engine is determined by previously set parameters such as pressure ratio and temperature ratio (see Table 6-1), there is no need to repeat the design point analysis because the engine is the same except for the fouled compressor section. To see the effect of fouling on overall performance, steady-state and transient performance analyses should be performed.

6.5.1 Steady-State Effects

To see the fouling effect on steady-state performance, generated fouled compressor map given in Figure 6-11 is used. The same methodology for a clean engine as explained in Chapter 3.1 has been applied to the fouled engine. For this purpose, 20 Beta lines are used, and the same turbine maps are introduced into the code in a tabulated form since this study aims to analyse only the compressor fouling effect.

As a result of fouling in 400 flight hours, the running line of the engine is shown on the compressor map in Figure 6-12.

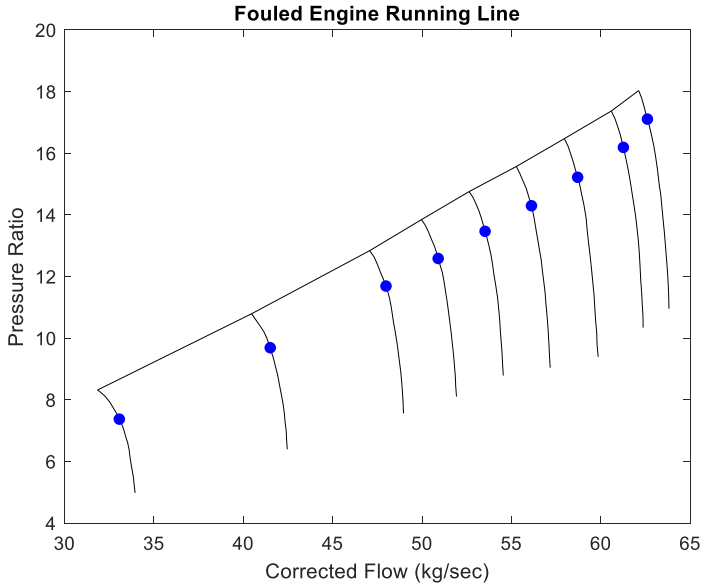

Figure 6-12 Engine Running Line with 400 Hr. Fouled Compressor – GE LM2500-30

For convenience, power outputs for engines with new and fouled compressors are given in Table 6-7.

Table 6-7 Power Values for Clean and Deteriorated Engines – GE LM2500-30

$\mathbf{N/\sqrt{\theta}}$	**Output Power with New Compressor** $(x10^3 kW)$	**Output Power with Fouled Compressor** $(x10^3 kW)$	**Difference Between Power Values (%)**
9450	22.65	20.42	9.85
9160	20.00	18.04	9.80
8971	17.73	15.95	10.04
8813	15.67	14.08	10.15
8660	13.96	12.55	10.10
8508	12.20	10.94	10.33
8364	10.51	9.43	10.28
8105	7.07	6.35	10.18
7772	3.93	3.58	8.91

It can be observed that steady-state power output values are degraded with the fouling. It can also be observed that for all the rotational speeds, the rate of change of degradation on power output is similar, so there is no characteristic difference in terms of power degradation level with rotational speed.

In addition to the power loss, another critical performance parameter, fuel consumption, shall be considered. For this analysis, the fouled engine is forced to deliver clean engine power under the same environmental conditions.

As expected, gas generator turbine spool speed also increases with the fuel flow rate. For this purpose, output power-gas generator speed and gas generator speed-fuel flow rate shall be modeled with fouled engine characteristics. The first relation between the output power and gas generator turbine speed is constructed using the fouled engine off-design steady-state results. The behavior of the gas generator turbine concerning the output power is approximated by using a 3rd order polynomial. The "poly3" function of MATLAB is used for this operation.

Then the curve equation is used to determine the gas generator turbine speed by introducing the clean engine output power as an input. Power values introduced to the equation are taken from the data given in Table 6-7. As a result of this operation, rotational speeds are found and listed in Table 6-8 at the desired power outputs.

Table 6-8 Generator Spool Rotational Speed Values at the Clean Engine Power Outputs – GE LM2500-30

Output Power ($x10^3 kW$)	**Clean Engine Ng (RPM)**	**Fouled Engine Ng (RPM)**	**Difference Between N_{ggt} Values (%)**
22.65	9450	9913	4.90
20.00	9160	9388	2.49
17.73	8971	9130	1.77
15.67	8813	8949	1.54
13.96	8660	8798	1.59
12.20	8508	8630	1.43
10.51	8364	8465	1.21
7.07	8105	8164	0.73
3.93	7772	7834	0.80

As can be deduced from Table 6-8, there is an increasing trend between the differences of the gas generator turbine rotational speed with the increasing power demand.

The next step for the analysis is to relate rotational speed and fuel flow rates. A similar operation is used to achieve fuel flow rates concerning rotational speed, and fouled engine operating data is approximated by a 3rd order polynomial.

Determination of the polynomial that gives the relation between rotational speed and fuel flow rate is followed by introducing the rotational speeds listed in Table 6-8. As a result of this analysis, fuel flow rates for the desired output powers are found and listed in Table 6-9.

Table 6-9 Fuel Flow Rates at the Clean Engine Power Outputs – GE LM2500-30

Output Power ($x10^3 kW$)	**Clean Engine Fuel Flow Rate (kg/sec)**	**Fouled Engine Fuel Flow Rate (kg/sec)**	**Difference Between Fuel Flow Rates (%)**
22.65	1.225	1.296	5.80
20.00	1.077	1.125	4.46
17.73	0.972	0.999	2.78
15.67	0.877	0.901	2.74
13.96	0.804	0.821	2.11
12.20	0.722	0.739	2.35
10.51	0.646	0.661	2.32
7.07	0.482	0.495	2.70
3.93	0.327	0.317	3.06

As seen in Table 6-9, there is an increase in the fuel flow rate as anticipated. Therefore, both gas generator turbine speed and fuel flow rates increase to deliver the same power with the engine having no fouling. In general, an engine with the FADEC system controls the fuel flow to maintain the output power. Therefore, instead of a decrease in engine power, fuel consumption increases.

6.5.2 Transient Effects

In order to observe the transient behavior of the engine under the effects of fouling, transient analysis explained in Chapter 4 is applied by using the fouled compressor performance map (given in Figure 6-11). Inertias are also kept the same for

compressor and turbine sections. Fuel flows obtained from the steady-state analysis (Chapter 6.5.1) are introduced in the step input form.

For ease of comparison, the response of the gas generator turbine with respect to time is given for both engines with clean and fouled compressors, respectively.

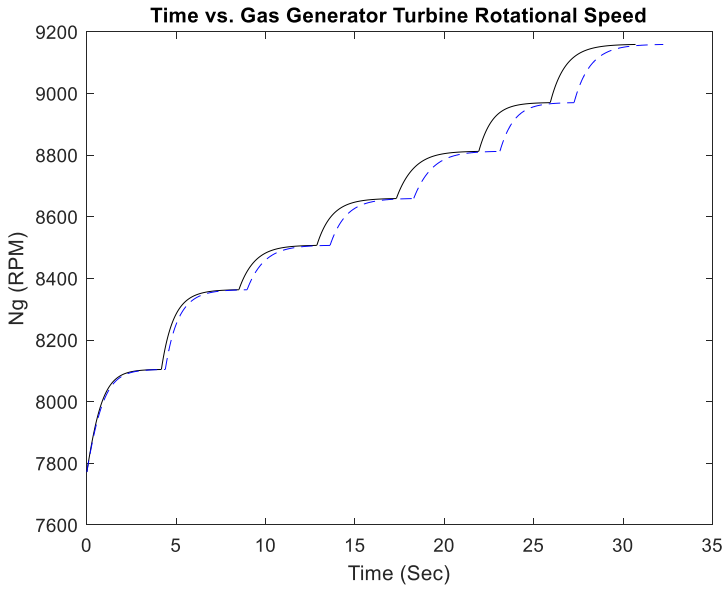

Figure 6-13 Clean (Black-Solid) vs Fouled (Blue-Dashed) Engine Gas Generator Turbine Speed Comparison – GE LM2500-30

In Figure 6-13, engine behavior is observed when the fuel is supplied to maintain the same gas generator turbine speed for each engine (fouled engine fuel flows are taken from the states where the engine runs on the line given in Figure 6-12). So that engines deliver different power outputs for the analysis performed to observe the transient response. The reason for considering the same rotational speed is to investigate the accelerating behavior of the engine.

Unlike the steady-state performance, there is a characteristic change with the varying speed (effect of degradation on power with the same speed does not vary much for different speeds, as given in Table 6-7). As deduced from Figure 6-13, while the engine compressor shaft rotational speed increases, the fouling effect becomes inevitable. Engine acceleration rate gets lower in contrast to the increase in speed.

At this point, it should be emphasized that there is no heat soakage model, and the control system is not integrated into the developed GE LM2500-30 engine model. Thus, the rate of change of referred speed, $Ndot$, is not controlled by any FADEC system. This means that the engine transient response varies with the level of deterioration. If there is a controller, fuel flow will be supplied to maintain the same acceleration/deceleration rate regardless of the deterioration level for a given operating condition [12]. The control algorithms and philosophies are well defined in [47], including the aforementioned $Ndot$ controlling logic.

In addition to the gas generator turbine response, engines are compared in terms of their gas generator turbine inlet temperatures which is one of the most important limiting factors of the engine performance. When the fuel flow amount is increased to move to the next step, a significant increase is seen in the turbine inlet temperature. Then this temperature peak is damped, and the engine reaches the steady-state value.

Therefore, fouled engine with a clean engine power output is used to compare engines in terms of temperature rise. The fuel flow data given in Table 6-9 are applied as step inputs. Gas generator turbine inlet corrected temperature behavior in response to the fuel inputs is considered. For convenience, the step that gives the power of the design point when convergence is achieved and presented in Figure 6-14.

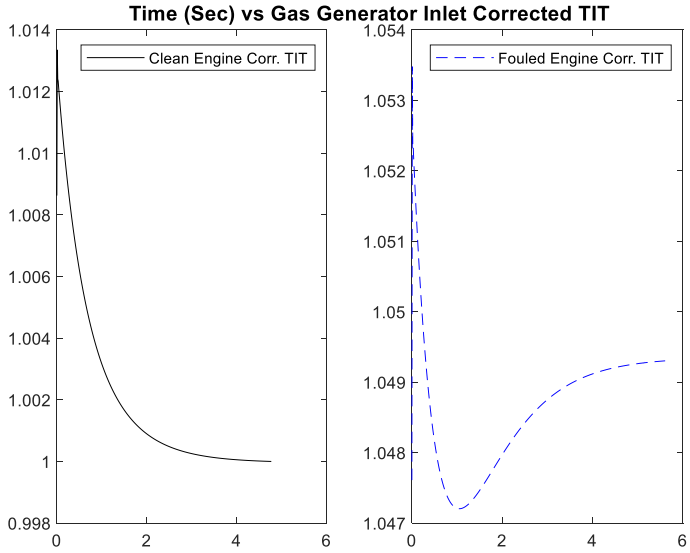

Figure 6-14 Gas Generator Turbine Inlet Temperature Variation in Response to Fuel Step Input – GE LM2500-30

In Figure 6-14, fuel flow input is introduced at time $t = 0$. As a result of the additional fuel flow, the temperature at the gas generator turbine inlet increases. Then, the temperature is damped, and the steady-state value is achieved. Unlike the gas generator turbine rotational speed response, the temperature reaches a higher value than required because of the sudden fuel addition. It can be concluded that the engine with a fouled compressor reaches higher temperatures at its peak, and also convergence temperature is higher by around 5% at this specific power output of 20MW. Convergence time is also higher for the fouled engine, as expected.

CHAPTER 7

CONCLUSIONS AND FUTURE WORK RECOMMENDATIONS

7.1 Conclusion

Throughout the study, it is aimed to develop a code that is capable of performing steady-state and transient performance analyses of the gas turbine. In addition to developing a code capable of performance analyses, a compressor map generation algorithm called the stage-stacking method is adopted and integrated into the developed code to overcome the limited data published by the manufacturers. Construction of the compressor map using the stage-stacking method is followed by the fouling application on the constructed map. With these capabilities of the developed code, engine preliminary design and investigations of deterioration effects on the performance are achieved.

In detail, the design of an engine is initiated by the design point analysis phase, which determines the engine's configuration. Design choices and limitations for the engine performance are set during this phase. High accuracy is required at this phase as it forms the basis of the design. An air model is developed and integrated to calculate the working fluid properties at the desired stations of the engine. After designing and integrating the air model, design point and parametric analysis modules are developed to compare different selections and choose the most optimum point for the engine's operation. The results of the design point and parametric study modules are compared with the commercial and widely used software called GasTurb 14 to ensure the reliability of the code. The comparison of results of developed code and GasTurb 14 verifies the development efforts.

The next step for engine design is performing off-design steady-state performance calculations. Throughout the off-design, the engine is analysed for varying operating

conditions with previously determined limitations and design parameters in the design point phase. So, performing the off-design calculations establishes the engine performance for all the steady-state operational behavior. In order to accomplish the off-design calculations, performance maps of the individual components are required in tabulated formats. For this reason, reference component maps are scaled according to the results of the design point analysis. The beta-line technique is applied to each component map to prevent erroneous calculations and achieve higher accuracy. Due to its robust and stable characteristics of the thermodynamic-matching algorithm, it is adopted through the calculations. The Newton-Raphson method is used for its fast and accurate nature. As a result of performing the off-design analysis of the engine, the engine's operating points with different gas generator turbine rotational speeds are obtained and compared with the GasTurb 14 outputs. Up to this point, the steady-state performance analysis of the engine is performed and verified with the GasTurb 14.

In addition to the steady-state analysis of the engine, transient behavior should be examined. In transients, there is a time-dependent change in performance parameters. In this module, the engine responses between steady-state thermal equilibrium points are considered, and fuel flows are introduced as step inputs to investigate the acceleration behavior of the engine. The effects of the polar moment of inertias are considered during the calculations. As for the steady-state analysis, Newton-Raphson Algorithm is used, and Euler Integration Method is considered for the matching and calculations for the next time step. The obtained results are also verified with the GasTurb 14 results.

After completing steady-state and transient performance analyses and the verification process of these modules, the developed code is validated by employing the GE T700 engine, which is widely used for validation purposes. For the steady-state model validation, fuel flows are changed, and converged points are considered. During the validation process of the model for the transients, fuel supply is suddenly

increased following the reference model. It is observed that results are in an acceptable range to accomplish the validation.

Developing the performance tool is then followed by integrating a compressor map generation algorithm called the stage-stacking method. Stage-stacking method is used to construct the detailed compressor performance map by considering the generalized characteristics of compressor stages. For the application of this method, only flow field geometry and running line data are required. Since these two data are available for the GE LM 2500-30, it is selected to be studied. The generation of the compressor map is followed by the inclusion of fouling effects on the performance parameters. For this purpose, a modified version of the method suggested by MacIsaac is used. After applying the method to the clean engine, fouled compressor performance map is constructed, and it is seen that performance parameters that are corrected flow rate, overall pressure ratio, and isentropic efficiency of the compressor section degrade.

Exhaustively, obtaining clean and fouled performance maps for the compressor section leads to the analysis of the performance effect of the compressor deterioration on the overall performance of the gas turbine. For this kind of analysis, developed code is used. The compressor section is already determined with the previously performed stage-stacking procedure during the design point phase by using literature data. Properties such as efficiency of the combustion chamber and turbine sections are assumed to match the results taken from the code with the data in the literature. Once the design point analysis is satisfactorily performed, turbine maps are scaled. Then the off-design analysis is initiated to see if the developed code is compatible with the running line data of the reference engine or not. Since the results are in close agreement with the clean engine running line data, engine response in the transient regime is considered. For this analysis, fuel flow rates are introduced as input, and gas generator turbine spool speed is examined for each fuel flow input. After these analyses, fouled compressor map and the same turbine maps used for the clean engine are used to examine the effects of compressor fouling on performance. For the fouled engine, it is not needed to perform design point analysis again since the

engine is the same except for the fouled compressor section. So, performance analysis begins with the off-design steady-state analysis. After applying the matching algorithm with the components, it is observed that engine output power degrades around 10% for almost every rotational speed. While performing this analysis, the same gas generator turbine rotational speeds are considered. Besides output power, fuel consumption is critical in terms of performance. Because of that, clean and fouled engines are compared in terms of fuel flow rates at the same output power. The fouled engine is forced to deliver clean engine power to compare fuel flow rates. At this analysis stage, fouled engine off-design running line data is used to derive the output power-gas generator turbine speed and gas generator turbine speed-fuel flow rate equations. Clean engine output power is delivered from both engines, and the gas generator turbine speed and fuel flow rate increase are observed on the fouled engine.

Comparative studies described until this point do not contain the engine's behavior concerning time. Because of that, responses in transient regime is considered for both clean and fouled engine. It is seen that fouled engine has lost its agility. In a more detailed manner, both engines are analysed at each individual off-design running line. So that the gas generator turbine spool speeds are the same for each engine, but fuel flow rates differ. When the engine accelerates to higher speeds, the convergence takes more time with the fouling effect. Since rotational speeds are already obtained for the same power outputs, it can be clarified that fouled engine response time is much longer than the clean engine.

Another parameter that should be examined with the gas generator turbine rotational speed is the turbine inlet temperature. Since the engine with a FADEC system schedules the fuel flow to prevent the over-temperature at the exit of the combustion chamber (i.e., gas generator turbine inlet), turbine inlet temperature becomes one of the limiting parameters. The same output powers are obtained from each engine to compare the clean and fouled engine in terms of temperature, and fuel flows are introduced for this purpose. It is seen from the analysis results that the corrected inlet

temperature of the gas generator turbine is approximately 4% higher at the peak for a design point condition. When the convergence is achieved, the corrected temperature of the fouled engine is approximately 5% higher. This means the engine deteriorates more easily, as these increased turbine inlet temperatures push the material limits at high rotational speeds. The FADEC system limits the supply of fuel to prevent this deterioration. This limitation brings the reduction in the delivered shaft speed or rate of acceleration to the desired state.

In conclusion, the fouled engine delivers less power at the same gas generator turbine speed. More fuel should be supplied to the engine to deliver the required power (delivered power values from the clean engine). At the same time, the gas generator turbine's rotational speed increases. An increase in both fuel flow and gas generator turbine rotational speed results in high-temperature operation, which will cause lifespan degradation.

7.2 Future Work Recommendations

Although the gas turbine performance analysis tool is developed and validated, it can be improved in terms of some of the aspects that are listed below:

- Control algorithm and control system reaction time for setting the power turbine rotational speed can be embedded,
- CO and NOx emission calculation modules can be added because of the environmental considerations,
- Heat soakage and inlet distortion calculations can be employed,
- A transient tip clearance model can be developed if the necessary data is available,
- Combustion delay models can be embedded,
- Engine starting control and scheduling module can be embedded to analyse the complete operation,

- Detailed component design modules (secondary air system, duct losses, mechanical offtakes, etc.) can be added to improve accuracy if detailed engine data is achievable.

REFERENCES

[1] Petrescu, R. V., Aversa, R., Akash, B., Bucinell, R., Corchado, J., Apicella, A., & Petrescu, F. I. (2017). Modern Propulsions for Aerospace-A Review. Journal of Aircraft and Spacecraft Technology.

[2] NASA Glenn Research Center. (2021, May 13). NASA. Retrieved from Ideal Brayton Cycle: https://www.grc.nasa.gov/www/K-12/airplane/brayton.html

[3] H. Saravanamuttoo, H. Cohen and G. Rogers, Gas Turbine Theory, Pearson Education Limited, 2001.

[4] Rolls-Royce plc. (2015). The jet engine. Wiley

[5] Ronald D. Flack. (2012). Fundamentals of Jet Propulsion with Applications. Cambridge University Press.

[6] Jack D. Mattingly. (2006). Elements of Propulsion: Gas Turbines and Rockets. American Institute of Aeronautics and Astronautics.

[7] AIRCRAFT GAS TURBINE ENGINES ENGINE TYPES And APPLICATIONS. (2001). Retrieved from Thai Technics: https://www.thaitechnics.com/engine/engine_type.html

[8] Kirk, D. (2016). Overview of Axial Compressors Retrieved from https://slideplayer.com/slide/7607189/

[9] Aerospace Notes. (n.d.). Retrieved from Aerospace Notes: https://aerospacenotes.com/classification-of-combustion-chamber/

[10] E.Winterbone, D. (1997). Combustion and flames. Advanced Thermodynamics for Engineers, 291-315.

[11] R.Noroozian, P.Asgharian. (2017). Chapter 4 - Microturbine Generation Power Systems. Distributed Generation Systems, 149-219.

[12] P. Walsh and P. Fletcher, (2004), Gas Turbine Performance, Oxford, UK: Blackwell Science Ltd.,

[13] SAE, (1996), Gas Turbine Engine Real Time Performance Model Presentation for Digital Computers, SAE Publication – ARP 4148, Society of Automotive Engineers, Warrandale, Pennsylvania.

[14] B. D. MacIsaac, H. I. H. Saravanamuttoo. (2015). A Comparison of Analog, Digital and Hybrid Computing Techniques for Simulation of Gas Turbine Performance. ASME 1974 International Gas Turbine Conference and Products Show.

[15] Thirunavukarasu, E.(2013). Modeling and Simulation Study of a Dynamic Gas Turbine System in A Virtual Test Bed Environment. (Master's thesis). Retrieved from https://scholarcommons.sc.edu/etd/2254

[16] J. Kurzke, (2022). GasTurb 14 Program and Manual. Germany.

[17] Kurzke, J., & Halliwell, I. (2018). Propulsion and Power An Exploration of Gas Turbine Performance Modeling. Springer International Publishing.

[18] Kurzke, J. (1995). Advanced User-Friendly Gas Turbine Performance Calculations on a Personal Computer. ASME Turbo Expo (Vol. 5).

[19] Kong, C., & Ki, J. (2001). Performance simulation of turboprop engine for basic trainer. ASME Turbo Expo (Vol. 2).

[20] Wemming, H. (2010). Validation and integration of a rubber engine model into an MDO environment. Linköping University.

[21] Martinjako, J. (2014). Low-Cost Gas Turbine Off-Design Prediction Technique (Master's Thesis), Arizona State University.

[22] Kong, C., Roh, H., & Lim, K. (2003, January). Steady-State and Transient Simulation of Turboprop Engine Using SIMULINK Model. ASME Turbo Expo (Vol. 3), 151-161.

[23] Kong, C., & Roh, H. (2003). Steady-state Performance Simulation of PT6A-62 Turboprop Engine Using SIMULINK. International Journal of Turbo and Jet Engines, 20, 183 - 194.

[24] Kuz'michev, V.S., Ostapyuk, Y.A., Tkachenko, A.Y., Krupenich, I.N., & Filinov, E.P. (2017). Comparative Analysis of the Computer-Aided Systems of Gas Turbine Engine Designing.

[25] Erk, M. (2015). Development of a cycle design software for turboshaft engines [M.S. - Master of Science]. Middle East Technical University.

[26] Mattingly, J. D., Heiser, W. H., & Pratt, D. T. (2002). Aircraft Engine Design. American Institute of Aeronautics and Astronautics Education Series.

[27] Ballin, Mark G. (1988). A high-fidelity real-time simulation of a small turboshaft engine. NASA Technical Memorandum.

[28] Uzol, O. (2011). A new high-fidelity transient aerothermal model for real-time simulations of the T700 helicopter turboshaft engine. Isi Bilimi Ve Teknigi Dergisi/ Journal of Thermal Science and Technology, 31(1), 37–44.

[29] Mihaloew, J. R., Selender, K., & Blaba, R. J. (1972). Generalized Simulation Technique for Turbojet System Analysis. NACA Technical Note.

[30] Szuch, J. R. and Bruton, W. M. (1976). Real-time simulation of the TF30-P-3 turbofan engine using a hybrid computer. NASA Technical Memorandum.

[31] Glassman, A. J. (1994). Turbine Design and Application. Retrieved from https://ntrs.nasa.gov/citations/19950015924

[32] Novikov, Y. (2012). Development of a high-fidelity transient aerothermal model for a helicopter turboshaft engine for inlet distortion and engine deterioration simulations [M.S. - Master of Science]. Middle East Technical University.

[33] Muir, D.E., Saravanamuttoo, H.I., & Marshall, D.J. (1989). Health Monitoring of Variable Geometry Gas Turbines for the Canadian Navy. Journal of Engineering for Gas Turbines and Power-transactions of the ASME, 111, 244-250.

[34] Howell, A. R., & Bonham, R. P. (1950). Overall and Stage Characteristics of Axial-flow Compressors. Proceedings of the Institution of Mechanical Engineers, 163(1), 235–248.

[35] General Electric. Gas Turbine Power Generation. (2018). Retrieved from: https://www.ge.com/power/gas/gas-turbines/lm2500.

[36] Mathioudakis, K., and Stamatis, A. (January 1, 1994). "Compressor Fault Identification from Overall Performance Data Based on Adaptive Stage

Stacking." ASME. J. Eng. Gas Turbines Power. January 1994; 116(1): 156–164

[37] Yang, H., & Xu, H. (2014). The New Performance Calculation Method of Fouled Axial Flow Compressor. The Scientific World Journal, 2014.

[38] Spina, P. R. (2002). Gas Turbine Performance Prediction by Using Generalized Performance Curves of Compressor and Turbine Stages. ASME Turbo Expo (Vol. 2 Parts A and B)

[39] Diakunchak, I. S. (April 1, 1992). Performance Deterioration in Industrial Gas Turbines. ASME. J. Eng. Gas Turbines Power. April 1992; 114(2): 161–168

[40] Meher-Homji, C. B., Chaker, M., & Bromley, A. F. (2009). The fouling of axial flow compressors - Causes, effects, susceptibility, and sensitivity. In Proceedings of the ASME Turbo Expo (Vol. 4, pp. 571–590).

[41] Rodríguez, C., Sánchez, D., Chacartegui, R., Muñoz, A., & Martínez, G. S. (2013). Compressor Fouling: A Comparison of Different Fault Distributions Using a "Stage-Stacking" Technique. In Proceedings of the ASME Turbo Expo (Vol. 2)

[42] Aker, G. F., and Saravanamuttoo, H. I. H. (April 1, 1989). Predicting Gas Turbine Performance Degradation Due to Compressor Fouling Using Computer Simulation Techniques. ASME. J. Eng. Gas Turbines Power. April 1989; 111(2): 343–350.

[43] Tarabrin, AP, Schurovsky, VA, Bodrov, AI, & Stalder, J. (1998). Influence of axial compressor fouling on gas turbine unit performance based on different schemes and with different initial parameters. In Proceedings of the International Gas Turbine & Aeroengine Congress & Exhibition (Vol. 4)

[44] MacIsaac, B. D. (1992). Engine performance and health monitoring models using steady state and transient prediction methods. Advisory Group for Aerospace Research and Development, AGARD-LS-183

[45] Seddigh, F., and Saravanamuttoo, H. I. H. (October 1, 1991). "A Proposed Method for Assessing the Susceptibility of Axial Compressors to Fouling." ASME. J. Eng. Gas Turbines Power. October 1991; 113(4): 595–601

[46] Tarabrin, A. P., Schurovsky, V. A., Bodrov, A. I., and Stalder, J. (April 1, 1998). "An Analysis of Axial Compressor Fouling and a Blade Cleaning Method." ASME. J. Turbomach. April 1998; 120(2): 256–261.

[47] Robinson, K. (1987). Digital Controls for Gas Turbine Engines In Proceedings of the International Gas Turbine Conference and Exhibition (Vol. 5)

APPENDICES

A. GE T700 ENGINE COMPONENT MAPS AND SCHEDULES

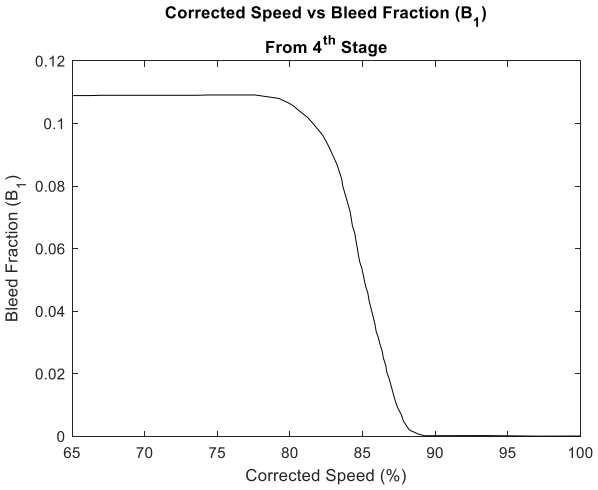

Figure A-1 4th Stage Bleed Fraction Relation for B_1[27]

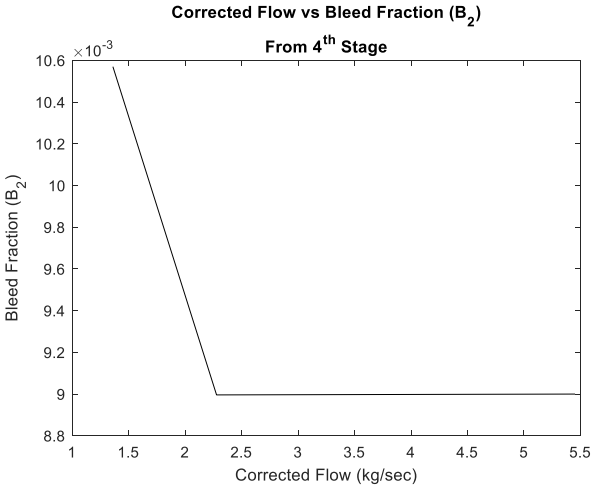

Figure A-2 4th Stage Bleed Fraction Relation for B_2[27]

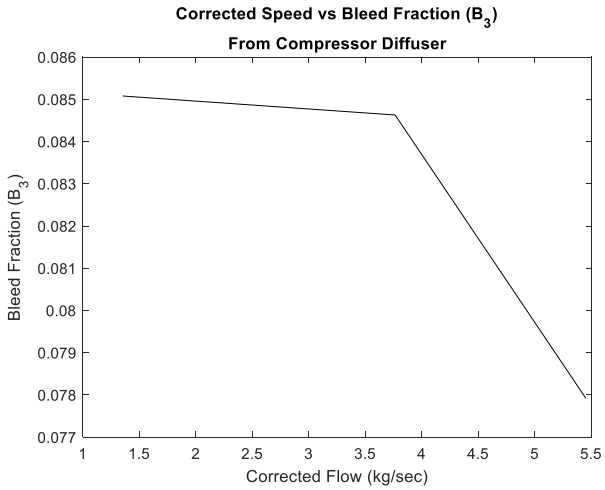

Figure A-3 Compressor Diffuser Bleed Fraction Relation for B_3[27]

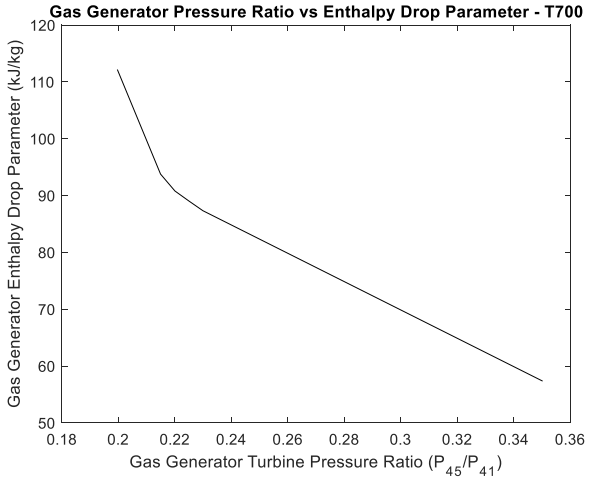

Figure A-4 Gas Generator Turbine Pressure Ratio and Enthalpy Drop Parameter Relation[27]

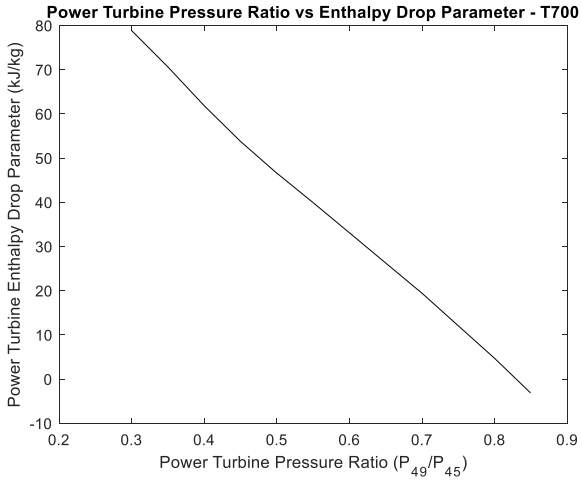

Figure A-5 Power Turbine Ratio and Enthalpy Drop Parameter Relation[27]

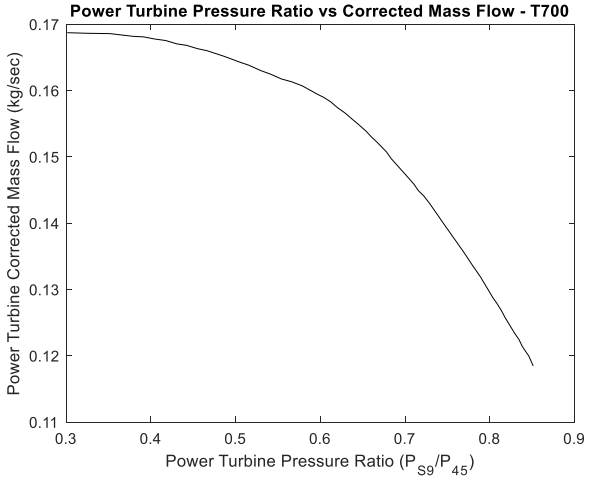

Figure A-6 Power Turbine Ratio and Corrected Mass Flow Relation[27]

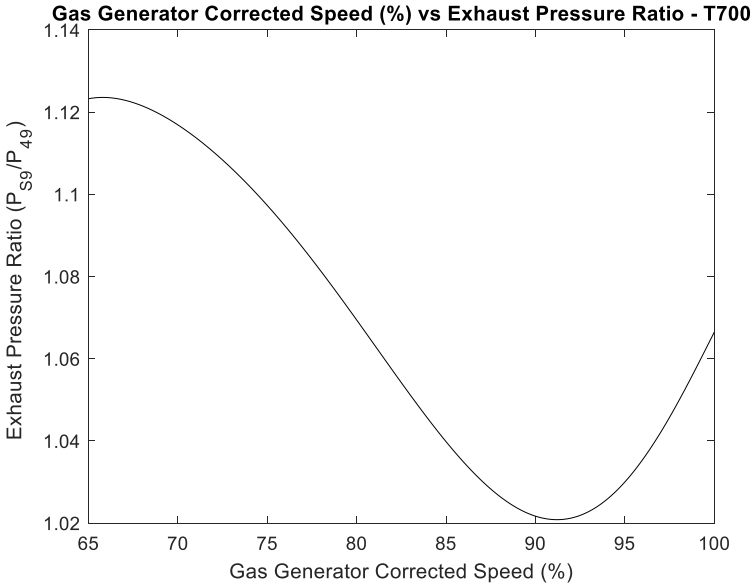

Figure A-7 Gas Generator Turbine Corrected Speed vs Exhaust Pressure[27]

B. STAGE-STACKING ALGORITHM